MIT Libraries | DSpace@MIT

MIT Open Access Articles

Membrane distillation model based on heat exchanger theory and configuration comparison

The MIT Faculty has made this article openly available. ***Please share*** how this access benefits you. Your story matters.

Citation: Swaminathan, Jaichander, Hyung Won Chung, David M. Warsinger, and John H. Lienhard V. "Membrane Distillation Model Based on Heat Exchanger Theory and Configuration Comparison." Applied Energy 184 (December 2016): 491-505.

As Published: http://dx.doi.org/10.1016/j.apenergy.2016.09.090

Publisher: Elsevier

Persistent URL: http://hdl.handle.net/1721.1/105758

Version: Author's final manuscript: final author's manuscript post peer review, without publisher's formatting or copy editing

Terms of use: Creative Commons Attribution-Noncommercial-Share Alike

Massachusetts Institute of Technology

Membrane distillation model based on heat exchanger theory and configuration comparison [1]

Jaichander Swaminathan, Hyung Won Chung, David M. Warsinger, John H. Lienhard V[2]

Rohsenow Kendall Heat and Mass Transfer Laboratory, Department of Mechanical Engineering, Massachusetts Institute of Technology, Cambridge MA 02139-4307 USA

Abstract

Improving the energy efficiency of membrane distillation (MD) is essential for its widespread adoption for renewable energy driven desalination systems. Here, an energy efficiency framework for membrane distillation modules is developed based on heat exchanger theory, and with this an accurate but vastly simplified numerical model for MD efficiency and flux is derived. This heat exchanger analogy shows that membrane distillation systems may be characterized using non-dimensional parameters from counter-flow heat exchanger (HX) theory such as effectiveness (ε) and number of transfer units (NTU). Along with the commonly used MD thermal efficiency (η), "MD effectiveness" ε should be used to understand the energy efficiency (measured as gained output ratio, GOR) and water vapor flux of single stage membrane distillation systems. GOR increases linearly with η (due to decreasing conduction losses), but increases more rapidly with an increase in ε (better heat recovery). Using the proposed theoretical framework, the performance of different single stage MD configurations is compared for seawater desalination. The gap between the membrane and the condensing surface constitutes the major resistance in both air gap (AGMD) and permeate gap (PGMD) systems (75% of the total in AGMD and 50% in PGMD). Reducing the gap resistance by increasing gap conductance (conductive gap MD (CGMD)), leads to an increase in ε through an increase in NTU, and only a small decrease in η, resulting in about two times higher overall GOR. GOR of direct contact MD (DCMD) is limited by the size of the external heat exchanger, and can be as high as that of CGMD only if the heat exchanger area is about 7 times larger than the membrane. While MD membrane design should focus on increasing the membrane's permeability and reducing its conductance to achieve higher η, module design for seawater desalination should focus on increasing ε by reducing the major resistance to heat transfer. A simplified model to predict system GOR and water vapor flux of PGMD, CGMD and DCMD, without employing finite difference discretization, is presented. Computationally, the simplified HX model is several orders of magnitude faster than full numerical models and the results from the simplified model are within 11% of the results from more detailed simulations over a wide range of operating conditions.

Keywords: Membrane Distillation Desalination, Energy Efficiency, Conductive Gap, Thermal Efficiency, Heat Exchanger, Performance Limits

[1]Citation: J. Swaminathan, H.W. Chung, D.M. Warsinger, and J.H. Lienhard V, "Membrane Distillation Model Based on Heat Exchanger Theory and Configuration Comparison, online 23 Oct. 2016, *Applied Energy*, 184:491-505, 15 Dec. 2016, http://dx.doi.org/10.1016/j.apenergy.2016.09.090

[2]Corresponding author: lienhard@mit.edu

Highlights

- GOR increases linearly with thermal efficiency, but more rapidly with effectiveness.
- Module design should increase overall heat transfer coefficient for seawater desalination.
- At constant flux and condenser area, GOR varies as AGMD < DCMD < CGMD.
- DCMD GOR exceeds CGMD only when heat exchanger area 7× greater than membrane area.
- Simplified heat-exchanger-theory based model for CG, PG and DCMD deviates <11%.

Nomenclature

Roman Symbols

A	Membrane area, m^2
$\bar{A}$	Ratio of heat exchanger area to MD membrane area
AGMD	Air gap membrane distillation
a_w	Activity of water
B	Membrane permeability, $kg/m^2 \cdot s \cdot Pa$
BPE	Boiling Point Elevation, °C
CGMD	Conductive gap membrane distillation
c_p	Specific heat capacity, J/kg·K
d	Depth or thickness, m
DCMD	Direct contact membrane distillation
dA	Elemental area, m^2
g	Gibbs free energy, J/kg
GOR	Gained Output Ratio
h	Heat transfer coefficient, $W/m^2 \cdot K$
h_{fg}	Enthalpy of vaporization, J/kg
HX	Heat exchanger
J	Permeate flux, kg/m^2 s
k	Thermal conductivity, W/m·K
L	Length of module, m
MD	Membrane distillation
MR	Ratio of cold permeate inlet mass flow rate to hot feed inlet flow rate in DCMD
$\dot{m}$	Mass flow rate, kg/s
NTU	Number of transfer units
P	Pressure, Pa
PGMD	Permeate gap membrane distillation
p^{vap}	Vapor pressure, Pa
$\dot{Q}$	Heat transfer rate, W
$\dot{q}$	Heat flux, W/m^2
Re	Reynolds number
RR	Recovery ratio
s	Salt concentration, g/kg
T	Temperature, °C
T_0	Ambient temperature, °C
TTD	Terminal Temperature Difference, °C
U	Overall heat transfer coefficient, $W/m^2 \cdot K$
v	Velocity, m/s
w	Width, m

Greek Symbols

δ_{m}	Membrane thickness, m
ε	Module effectiveness
η	MD thermal efficiency
ϕ	Membrane porosity
ρ	Density

Subscripts/Superscripts

b	Stream bulk
br	Brine stream
c	Cold stream
ch	Cold or hot flow channel
f	Feed (hot) stream
g	Gap
h	Heater
in	Inlet
m	Membrane surface
out	Outlet
p	Product stream
s	Solid
sat	Saturation
v	Vapor
wall	Condensing surface

1. Introduction

Increasing unmet demand for water, due to rising population and rising consumption rates, is leading to increasingly wide-spread use of desalination as an alternative source of water, with installed capacity now above 85 GL/day [1]. Desalination involves the separation of pure water from a saline stream, often the ocean, but frequently ground water. The separation of pure water is achieved either by the application of mechanical work, in the form of pressure in the case of reverse osmosis, or electricity in the case of electrodialysis, or by the use of thermal energy through phase change as in multi-effect distillation, multi-stage flash distillation, freeze desalination, etc. Even when carefully optimized, desalination is an energy-intensive process and hence many investigators have looked towards offsetting the energy requirement through renewable energy resources. Solar thermal energy or geothermal energy can be used for thermal desalination. Similarly, renewable electricity production has been used to reduce the carbon-footprint of reverse osmosis or electrodialysis systems.

Membrane distillation (MD) is a thermal desalination process that is particularly interesting for renewable energy applications because it can use low temperature, low grade heat sources. The process is very simple, requiring no high-pressure or vacuum pumps leading to a modular scalable system. Ghaffour et al. [2] recently investigated membrane distillation and adsorption desalination as innovative energy efficient desalination options for combining with renewable energy sources. Sarbatly and Chiam [3] evaluated MD powered by geothermal energy and found that while cost of water from a vacuum MD system powered from conventional sources is about US\$1.29/m^3, with geothermal energy use, the cost drops to about US\$0.5/m^3 making it competitive with other desalination technologies.

Suarez et al. [4] investigated low-temperature direct contact membrane distillation in combination with a solar thermal gradient salt pond. About 70% of the total energy collected was used within the MD module, but sensible heat conduction losses through the membrane made up 50% of this energy. The study's authors identified the need to reduce heat losses and improve the thermal efficiency of the process in order to make solar-powered renewable desalination viable.

Another relevant question associated with renewable MD systems is the choice of MD configuration. Zaragoza et al. [5] investigated this by experimentally comparing five commercial MD modules in air gap, permeate gap, and multi-effect vacuum configurations for desalination coupled with solar thermal energy. Although the recovery ratio, defined as pure water production divided by feed flow rate, of the multi-effect system can be an order of magnitude higher than for single stage configurations, the energy efficiency of single stage spiral wound permeate gap systems was the maximum. Electrical energy consumption for maintaining the vacuum was also significant in the case of the multi-effect vacuum configuration.

The recurring challenges in the above studies are the low energy efficiency of membrane distillation preventing MD's widespread use for renewable desalination and the various MD configurations being pursued without a clear hierarchy in terms of their energetic performance. In this article, multiple membrane distillation configurations are investigated under similar conditions to compare their energy efficiency and capital cost. In any given single stage MD configuration, there is a trade-off between energy efficiency and capital costs, with energy costs decreasing and capital expenditure increasing with larger module length. In the present work, a clear trend is established in terms of overall performance and cost among different MD configurations. The similarity between MD and heat exchangers is recognized and used to develop a simple theory to explain MD performance metrics. In addition, numerical models are developed for direct contact, permeate and conductive gap MD systems based on this theory. These can be utilized without large computational or experimental expenditure. These results will hasten the development of optimized MD systems for renewable desalination applications.

1.1. Membrane distillation configurations

Most studies on MD start by listing four different configurations of membrane distillation in the introduction, before choosing to focus on one of these configurations. The different configurations vary based on how the vapor that passes through a hydrophobic membrane is condensed and collected as pure liquid water and also how this condensation energy is recovered [6]. As a result, this choice has significant influence on the overall energy efficiency and cost of the process [7].

Direct contact membrane distillation (DCMD) is the oldest configuration [8], with cold pure water receiving and immediately condensing the vapor on the other side of the membrane. The vapor is carried

out of the module and condensed externally in the vacuum and sweeping gas configurations. In the air gap membrane distillation configuration (AGMD), condensation occurs inside the module, within an air gap between the membrane and the condensing surface. The feed water acts as the coolant enabling direct heat recovery within the module [9, 10]. This eliminates the external heat exchanger that needs to be used in the case of DCMD to transfer the energy from the pure water leaving the MD module to the incoming feed.

The energy efficiency of a single stage vacuum MD system is low, necessitating multi-staging for performance improvement [11, 12, 13, 14]. A single stage sweeping gas MD is thermodynamically similar to a humidification dehumidification desalination system and so is restricted to low energy efficiency values without staging or extraction [15]. AGMD and DCMD on the other hand, can potentially achieve higher energy efficiency in a single stage system [11] and hence will be considered in this study.

More recently, several novel MD configurations with modified gaps have been proposed in the literature, including permeate gap membrane distillation (PGMD) [16, 17] where the gap region is filled with pure condensate, material gap membrane distillation with additional substances such as sand added to the gap [18] as well as conductive gap membrane distillation (CGMD) with high rather than low overall conductance of the gap region [19, 20]. Swaminathan et al. [20] showed that CGMD outperforms PGMD by about two times in terms of GOR, and that PGMD itself can have about 10% higher GOR than AGMD.

1.2. Outline

In Section 1, existing membrane distillation efficiency parameters such as energy efficiency or gained output ratio (GOR), η (MD thermal efficiency), and flux (J) are reviewed. The finite difference numerical model used in this study is reviewed.

Effectiveness (ε) is introduced in Section 2 as an additional useful parameter to understand MD energetic performance. The energy efficiency of single stage MD systems with internal heat recovery is derived in terms of η and ε. Using this expression, an upper limit for MD's GOR is evaluated and compared to the thermodynamic limit for a generic thermal desalination system.

The literature has mostly focused on the importance of reducing conduction losses through the membrane (increasing η). In Section 3, the relatively higher importance of achieving better heat recovery within the module (or higher effectiveness ε) is illustrated. The theory developed in the previous sections is used to understand the trend of increasing GOR observed in PGMD and CGMD with improving gap conductance, for desalination of seawater.

In Section 4, the GOR of DCMD is derived in terms of η and ε and the properties of the external heat exchanger, to enable comparison with other configurations with internal heat regeneration. The inherent disadvantage of using an additional external heat exchanger in DCMD is quantified through the $\mathrm{TTD}_{\mathrm{factor}}$. This parameter is a function of the terminal temperature difference (TTD) of the MD and the heat exchanger (HX). The GOR of DCMD is lower than that of CGMD when the external heat exchanger area is equal to the membrane area. If the relative size of the heat exchanger is increased, DCMD performance approaches and eventually marginally exceeds that of CGMD.

In Section 5, the magnitude of the various internal heat transfer resistances are compared for the various configurations. The gap between the membrane and the condensing surface constitutes the major resistance in AGMD and PGMD, whereas the flow channel and the membrane resistances are important in the case of DCMD and CGMD. Using this framework, the effects of increasing membrane permeability and flow channel heat transfer coefficients are analyzed.

Finally, in Section 6, a simplified model for evaluating the performance of PGMD and CGMD systems without employing finite-difference or other discretization techniques is presented. The model is inspired by the ε-NTU (number of transfer units) method for heat exchangers, recognizing the similarity between a well-designed MD system and a counter-flow heat exchanger. ε and η are rewritten in terms of the effective transport resistances within the MD module, and so the GOR and flux of an MD system can be evaluated given the geometrical parameters of the system and the input conditions such as feed flow rate and heater outlet temperature. This simplified model is intuitive and computationally orders of magnitude faster than discretization based methods, while producing results within 10% of the more complicated models over a wide range of operating conditions.

1.3. MD efficiency parameters

MD thermal energy efficiency is expressed as a gained output ratio (GOR). A higher GOR indicates lower thermal energy consumption. While thermal energy constitutes the major part of the cost of water from MD, capital costs may also be significant. The performance parameter relevant to capital cost is the flux of water through the membrane, which quantifies the membrane productivity. Higher flux results in lower capital cost of the MD process. Some of these existing efficiency metrics for MD are reviewed in this section.

1.3.1. Gained output ratio

The overall system energy efficiency is measured as a non-dimensional parameter, gained output ratio (GOR):

$$\mathrm{GOR} = \frac{\dot{m}_{\mathrm{p}} h_{\mathrm{fg}}}{\dot{Q}_{\mathrm{h}}} \tag{1}$$

where $\dot{m}_{\mathrm{p}}$ is the rate of permeate production, h_{fg} is the enthalpy of evaporation and $\dot{Q}_{\mathrm{h}}$ is the power input in the heater. GOR is the inverse of specific thermal energy consumption times the enthalpy of vaporization of water. A higher value of GOR corresponds to a lower thermal energy consumption per unit mass of distillate. A value of 1 corresponds to a system with no losses and no condensation energy recovery. In practice, multiple energy losses occur, such as the disposal of hot brine or heat conduction through the walls of the system, and so a system without condensation energy recovery would have GOR much lower than 1. In contrast, large scale thermal desalination plants such as multi-stage flash and multi-effect distillation systems may have GOR of about 10.

A large majority of membrane distillation studies have been performed on a small scale without energy recovery, and hence do not discuss GOR. Summers and Lienhard [21] performed a detailed analysis to scale AGMD performance as a function of system size. Summers et al. [11] reported GOR of AGMD and DCMD systems of about 5-6 based on numerical modeling. They showed that GOR increases with an increase in channel heat transfer coefficient, membrane area, top temperature or bottom temperature. At larger specific membrane area $\left(= \frac{A}{\dot{m}_{\mathrm{f}}}\right)$, Summers et al. found that AGMD achieves the highest GOR, whereas at lower areas, DCMD achieves higher GOR. This result was based on a fixed external heat exchanger TTD=3 °C for the DCMD module. The feed and cold stream input flow rates were also set to be equal in this study, and hence there is scope for improvement by balancing the DCMD operation.

Zuo et al. [22] analyzed the GOR and cost of a cross-flow hollow fiber DCMD module. Gilron et al. [23] analyzed a cascade of cross-flow DCMD modules, where increasing the number of stages is similar to increasing the length of a flat sheet countercurrent MD system. A GOR of about 9.5 was reported for an 11-stage system with a top temperature of 95 °C. Lin et al. [24] report the specific thermal energy consumption of DCMD as a function of MR (ratio of distillate and feed input mass flow rates) and membrane permeability. Over the range of membrane permeability considered, they found that the maximum GOR varies from about 1.5–10.

He et al. [25] and Geng et al. [26] have reported high experimental values for GOR for hollow fiber AGMD. The maximum GOR reported in [26] is 8.8 at hot and cold temperatures of 90 and 40 °C and feed NaCl salinity of 35 g/kg.

Zaragoza et al. [5] compared the performance of several commercial MD modules in permeate gap, air gap and multi-effect vacuum configurations. While multi-effect vacuum MD achieved much higher recovery ratio, spiral wound single stage systems achieved the highest energy efficiency and similar permeate flux as the multi-effect system.

1.3.2. Flux

Pure water flux J, often measured in L/m^2 h or LMH is the subject of significant investigation in the membrane distillation literature. Flux can be expressed as:

$$J = \frac{\dot{m}_{\mathrm{p}}}{A} \times 3600 \left[\frac{\mathrm{s}}{\mathrm{hr}}\right] \times \frac{1}{\rho \left[\frac{kg}{L}\right]} \tag{2}$$

where A is the area of membrane in m^2 and ρ is the density of the feed stream in kg/L.

DCMD has the highest flux, and AGMD has much lower flux, for coupon scale experiments. A coupon sized experiment is where the hot and cold stream temperatures do not change significantly along the flow direction between the entrance and exit of the module. As a result, lower mass transfer resistance in DCMD directly corresponds to a higher flux.

While the flux in coupon sized experiments can be higher than 100 LMH, in a real MD system with heat regeneration, the driving temperature difference across the membrane is lower and hence fluxes are more modest at about 5 LMH.

The trade-off between flux and GOR was recognized for hollow fiber DCMD in [23], with GOR increasing with stages, but flux decreasing. Several other researchers have recognized this trade-off and some have used flux vs. GOR plots to visualize the same [25, 27].

Under coupon scale systems, the flux with PGMD has been shown to be higher than that of AGMD [17, 18]. Recently, CGMD was shown to have four times higher flux than AGMD for a gap thickness of about 3 mm [20]. Tian et al. [28] also performed coupon-sized experiments under CGMD conditions by allowing partial contact between the membrane and the condensing surface and achieved better mixing of the feed stream. The flux under this condition was 120 LMH with $T_{\mathrm{f}} = 77\,^{\circ}\mathrm{C}$ and $T_{\mathrm{c}} = 12\,^{\circ}\mathrm{C}$. In a larger system with energy recovery, it is shown that the flux of PGMD and CGMD are likely to of similar magnitude [20] or even lower than that of AGMD for the same membrane area (Fig. 8b).

Wu et al. [29] recently developed a heat-exchanger (ε-NTU) model to evaluate the flux of DCMD. The model is applicable for both parallel and counterflow configurations at low feed salinity and operates at small computational cost compared to finite difference methods. Since an overall heat transfer coefficient defined between the feed and cold bulk streams is used, a correction factor was additionally used to enhance the accuracy of the model by increasing the relative importance of the heat transfer coefficient on the hot side over the cold side.

1.3.3. Thermal efficiency

Thermal efficiency (η) of membrane distillation is defined as the fraction of the energy transferred from the hot side by mass transfer. For a system with little or no condensation energy recovery, η is the most important efficiency parameter of interest. In the ideal scenario, all the heat supplied to the MD process should be used for evaporation and should not be leaked from the hot side to the cold side as heat conduction losses. This ideal case would correspond to a thermal efficiency of 1. However, even with a membrane material that is perfectly insulating, η cannot reach 1 due heat conduction through the vapor [24]. Nevertheless, $\eta = 1$ is a useful upper limit to consider. Formally, η may be defined as follows:

$$\eta = \frac{\dot{Q}_{\mathrm{mass}}}{\dot{Q}_{\mathrm{tot}}} = \frac{\dot{Q}_{\mathrm{mass}}}{\dot{Q}_{\mathrm{mass}} + \dot{Q}_{\mathrm{cond}}} \tag{3}$$

where, $\dot{Q}_{\mathrm{mass}}$ is the heat transfer rate associated with vapor transport through the membrane, which can be evaluated as the area weighted sum of the heat flux ($\dot{q}$) as:

$$\dot{Q} = \int_A \dot{q}\, dA \tag{4}$$

where the integral is evaluated over the total area of the membrane. The heat flux at any local section along the length of the module is a function of the membrane permeability (B) and vapor pressure difference across the membrane (Δp_{vap}), given by:

$$\dot{q}_{\mathrm{mass}} = B \cdot \Delta p_{\mathrm{vap}} h_{\mathrm{fg}}(T_{\mathrm{g,m}}) \tag{5}$$

Similarly, $\dot{Q}_{\mathrm{cond}}$ refers to the conduction heat transfer rate through the membrane and is based on the local heat conduction flux given by

$$\dot{q}_{\mathrm{cond}} = \frac{k_{\mathrm{m}}}{\delta_{\mathrm{m}}} \left(T_{\mathrm{f,m}} - T_{\mathrm{g,m}}\right) \tag{6}$$

where k_{m} is the effective conductivity of the membrane, δ_{m} is the thickness of the membrane and $T_{\mathrm{f,m}}$ and $T_{\mathrm{g,m}}$ are the temperatures at the feed-membrane and gap-membrane surfaces.

Membrane design should focus on increasing porosity and reducing membrane material conductivity to achieve high η [30]. There are clear differences in η between various MD configurations. DCMD has the lowest η among MD configurations. The presence of the additional air layer, with a much lower conductivity, leads to a larger η in the case of AGMD. Although the overall effective permeability and hence flux is lower in the case of AGMD, the fraction of heat transferred through conduction is also lower, leading to higher η. Ali et al. [31] analyzed the effect of various membrane properties on the cost of water production from a small-scale MD system and found that while DCMD costs were affected by membrane conductivity and thickness, AGMD was relatively unaffected. This can be explained based on the trends in η discussed previously.

The value of η for MD systems has often been measured in coupon sized systems with relatively high flux. A wide of range of values have been reported for η, ranging from 0.2 to 0.95. In AGMD, the presence of the air gap ensures that $\eta > 0.85$ [32]. For DCMD, in contrast, η can vary over the wide range as a function of membrane properties and operating conditions. For low permeability membranes [33], or at high feed salinity [34], η can be quite low [35] . On average, η is greater than about 50–60% [27, 36, 37, 38, 39], and for well-designed membranes η can be quite high at about 0.75–0.85 [40, 41, 42, 43]. The discussion in Section 6 can help explain this wide range in the observed values.

For larger systems with significant energy recovery, GOR is directly affected by η. Fane et al. [44] expressed the GOR of DCMD as:

$$\mathrm{GOR}_{\mathrm{DCMD}} = \eta \times \frac{\Delta T_{\mathrm{MD}}}{\mathrm{TTD}_{\mathrm{MD}} + \mathrm{TTD}_{\mathrm{HX}}} \tag{7}$$

where ΔT_{MD} is the axial temperature change of the feed as it flows through the MD module. This expression has been used subsequently by several other investigators [22, 23].

Koschikowski et al. [45] expressed GOR of a system with internal heat regeneration, such as PGMD, AGMD, and CGMD, as a function of η in the form:

$$\mathrm{GOR} = \eta \times \frac{T_{\mathrm{c,out}} - T_{\mathrm{c,in}}}{T_{\mathrm{f,in}} - T_{\mathrm{c,out}}} \tag{8}$$

Guan et al. [27] proposed an implicit expression linking GOR and η based on measured permeate and feed flow rates.

1.4. Modeling

The modeling results presented in this study are based on the one-dimensional finite difference numerical modeling framework presented in [11, 20]. The variations in parameters such as flow rate, temperature and salinity along the module length are modeled along with the effect of heat and mass transfer boundary layers. All the results are presented for 'balanced' system conditions with highest efficiency. Balancing is achieved based on the principle of thermodynamic equipartition presented in Thiel et al. [46]. In the case of PGMD, CGMD and AGMD, balance refers to the condition where the pure water in the gap flows in the same direction as the feed water [20]. In the case of DCMD, balance refers to the condition where the heat capacity rates of the two streams are equal [24, 47]. The validation of the model against experimental data from large-scale MD systems is presented in Appendix A.1.

2. MD energy efficiency theory

2.1. GOR as a function of MD effectiveness, ε

Figure 1 shows schematic diagrams of the MD configurations considered in this study and the various temperatures are labeled. The flux of CGMD is higher than that of PGMD for coupon-sized systems. For a larger scale system designed for high GOR, Swaminathan et al. [20] showed that the higher GOR of CGMD compared to PGMD is not because of improved flux, but rather an effect of better energy recovery within the module [20]. Better energy recovery within the module leads to a higher temperature of the preheated stream, leading to lower external heat input and hence higher GOR. In this context, another parameter, the MD system effectiveness, ε is defined here. Adapted from two-stream heat exchanger theory, ε compares the actual change in enthalpy of the cold stream to the maximum possible change in enthalpy of the cold

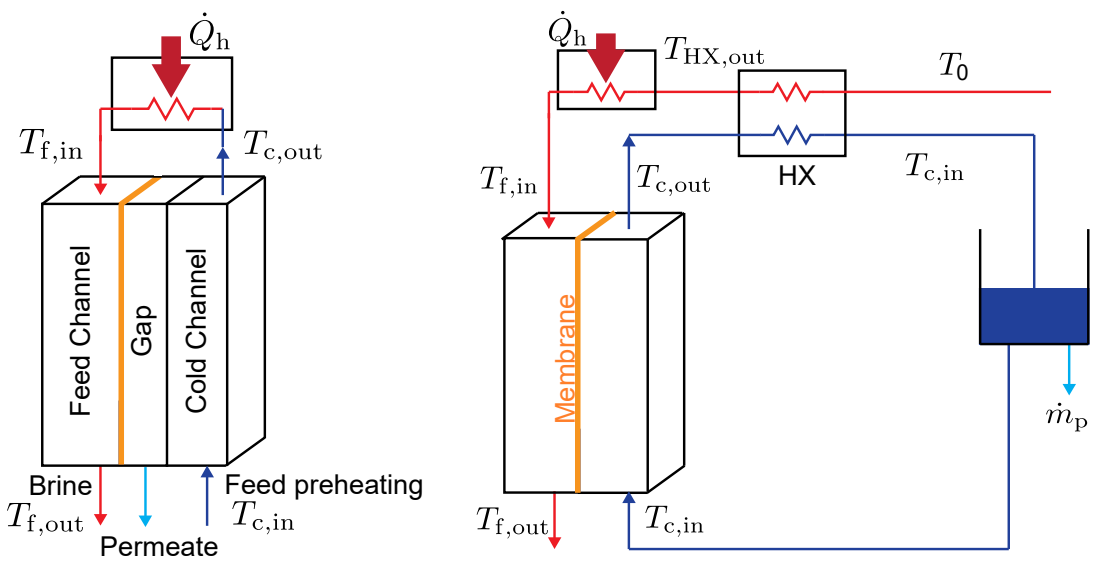

(a) AGMD, PGMD or CGMD.

(b) DCMD system.

Figure 1: Schametic diagrams of MD systems.

stream. The specific heat capacity is relatively constant over the range of temperatures considered, so the equation may be reduced to a ratio of temperature differences:

$$\varepsilon = \frac{h_{c,out} - h_{c,in}}{h_{f,in} - h_{c,in}} = \frac{T_{c,out} - T_{c,in}}{T_{f,in} - T_{c,in}} \tag{9}$$

The cold stream is an ideal choice for defining ε since the mass flow rate and salinity of the cold stream are constant along the length of the module (for PGMD, CGMD, and AGMD).

ε is therefore a measure of energy transfer between the hot and cold streams scaled by the total possible energy transfer, and a value of $\varepsilon = 1$ corresponds to an infinite area MD heat exchanger where the cold stream leaves at the hot inlet temperature and vice versa.

The GOR of AGMD, PGMD and CGMD can be expressed in terms of η and ε as follows:

$$\begin{aligned} \text{GOR} &= \frac{\dot{m}_p h_{fg}}{\dot{Q}_h} \\ &\approx \frac{\dot{Q}_{mass}}{\dot{Q}_h} \\ &= \eta \times \frac{\dot{Q}_{total}}{\dot{Q}_h} \\ &= \eta \times \frac{T_{c,out} - T_{c,in}}{T_{f,in} - T_{c,out}} \\ &= \eta \times \frac{\varepsilon}{1 - \varepsilon} \end{aligned} \tag{10}$$

where $\dot{Q}_{total}$ is the total heat transferred from the hot stream to the cold stream and $\dot{Q}_{mass}$ is the heat transfer associated with vapor transfer across the membrane. The numerical values of GOR evaluated using Eqs. 1 and 10 may differ slightly based on the temperature at which h_{fg} is evaluated in Eq. 1, since in Eq. 10 an average value of h_{fg} within the module is used.

From Eq. 10, GOR increases non-linearly with an increase in ε, whereas the dependence on η is linear. This expression will be used to understand the effect of increasing the gap conductivity in next section.

2.2. Deriving an expression for the upper limit of MD GOR

The maximum possible efficiency for MD systems can be derived from the new expression for MD GOR with ε, Eq. 10, and using the limitation of boiling point elevation.

Mistry et al. [48] analyzed the maximum performance limit for a general thermal desalination system with heat supply from a source at T_{h} and environment temperature T_0 by setting entropy generation equal to zero as:

$$\begin{aligned}\mathrm{GOR}^{\mathrm{limit}}_{\mathrm{thermodynamic}} &= \frac{h_{\mathrm{fg}}}{\frac{\dot{Q}_{\mathrm{h,least}}}{\dot{m}_{\mathrm{p}}}} \\ &= \frac{h_{\mathrm{fg}}\left(1-\frac{T_0}{T_{\mathrm{h}}}\right)}{g_{\mathrm{p}}+\left(\frac{1}{\mathrm{RR}}-1\right)g_{\mathrm{br}}-\frac{1}{\mathrm{RR}}g_{\mathrm{f}}}\end{aligned} \tag{11}$$

where g is the Gibbs energy, RR is the recovery ratio or ratio of pure product production to feed input, T_{amb} is the ambient temperature and T_{h} is the temperature of the heat source in the heater.

The least heat of separation for pure water is zero [49], corresponding to a maximum achievable GOR approaching ∞. At higher input salinities, the denominator increases and hence the maximum achievable GOR is lower.

For a single stage MD system, the GOR predicted by Eq. 10 should be lower than this thermodynamic limit. For an infinite area MD system, $\varepsilon \to 1$ so that GOR $\to \infty$ if $\eta > 0$. This is possible when the feed is pure water; with real solutions, boiling point elevation makes approaching ε of one impossible. When the feed is salt water of salinity s_{f}, in order to sustain positive fluxes within the module, the feed and cooling fluid temperature difference at the membrane surface ($T_{\mathrm{f,m}} - T_{\mathrm{c,m}}$, at any local position within the module) should be greater than the local value of boiling point elevation ($BPE\left(T_{\mathrm{f,m}}, s_{\mathrm{f,m}}\right)$) [13]. At infinite area, flux is very close to zero, leading to near zero temperature and concentration polarization ($T_{\mathrm{f,m}} \approx T_{\mathrm{f,b}}$, $T_{\mathrm{c,m}} \approx T_{\mathrm{c,b}}$), and hence only the membrane offers resistance to transport. The minimum temperature difference between the bulk streams in MD and heat exchangers occurs at one end of the system and can be defined as the terminal temperature difference (TTD). TTD would have to be at least greater than or equal to the maximum BPE within the module to sustain positive vapor flux within the system (i.e., $\mathrm{TTD}_{\mathrm{min}} = \mathrm{BPE}_{\mathrm{f,in}}$). To understand the upper bound for GOR, an effective membrane thermal conductivity of 0 W/m-K is assumed by setting $\eta = 1$. In reality, even if the membrane is extremely porous, the lower limit for effective thermal conductivity is $k_{\mathrm{air}} \approx 0.02$ W/m-K, leading to $\eta < 1$.

ε can be expressed as a function of module TTD $= T_{\mathrm{f,in}} - T_{\mathrm{c,out}}$, using Eq. 9 as

$$\varepsilon = 1 - \frac{\mathrm{TTD}}{T_{\mathrm{f,in}} - T_{\mathrm{c,in}}} \tag{12}$$

Equation 10 can then be rearranged as

$$\mathrm{GOR} = \eta\left(\frac{T_{\mathrm{f,in}} - T_{\mathrm{c,in}}}{\mathrm{TTD}} - 1\right) \tag{13}$$

The upper bound for GOR can therefore be expressed by substituting $\mathrm{TTD}_{\mathrm{min}} = \mathrm{BPE}_{\mathrm{f,in}}$ and $\eta = 1$ as

$$\mathrm{GOR}_{\mathrm{limit,MD}} = \frac{T_{\mathrm{f,in}} - T_{\mathrm{c,in}}}{\mathrm{BPE}_{\mathrm{f,in}}} - 1 \tag{14}$$

The two functions (Eqs. 11, 14) are plotted as a function of input salinity in Fig. 2. A recovery ratio (RR) of 10.11% is used for evaluating the thermodynamic limit since that is the average recovery ratio with an infinite area MD system with zero heat conduction across the membrane over the range of input salinities considered. The seawater property package of Sharqawy et al. and Nayar et al. ([50, 51]) is used to evaluate the Gibbs energy and boiling point elevation of seawater at various salinities and temperatures.

As seen in Fig. 2, $\mathrm{GOR}_{\mathrm{max,MD}}$ is bounded by $\mathrm{GOR}_{\mathrm{max,thermodynamic}}$. One reason for lower $\mathrm{GOR}_{\mathrm{max,MD}}$ is that the boiling point elevation varies along the module length. As a result, vapor flux is driven by a non-zero driving force, generating entropy elsewhere. Both η and ε are lower for real MD systems since the membrane is not a perfect insulator and the area of the system is finite. As a result, real GOR values are at least an order of magnitude lower than the maximum possible GOR, leading to a second law efficiency of less than 10% as observed by Mistry et al. [52].

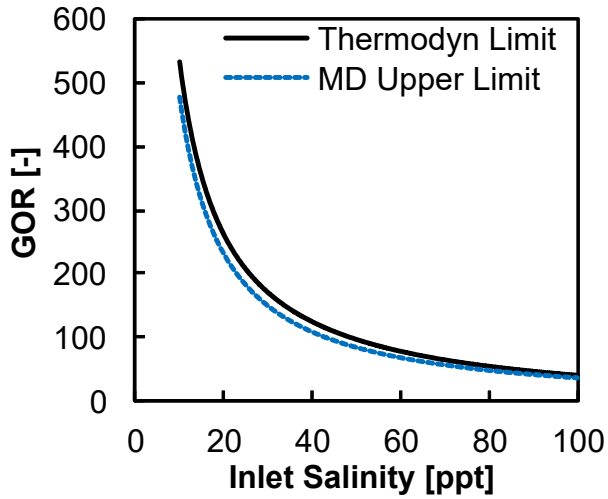

Figure 2: Limits of MD system energy efficiency

3. MD configuration comparison

Results are presented based on a Millipore ISEQ00010 PVDF membrane with an average pore size of 0.2 μm, porosity of 80% and thickness of 200 μm. The B value for this membrane at $T_{\mathrm{f}} = 60°\mathrm{C}, T_{\mathrm{c}} = 20°\mathrm{C}$ is measured as 16×10^{-7} kg/m^2-s-Pa. At higher temperatures, B was higher (20×10^{-7} kg/m^2-s-Pa at $T_{\mathrm{f}} = 70°\mathrm{C}$) and at lower temperatures the value was lower (12×10^{-7} kg/m^2-s-Pa at $T_{\mathrm{f}} = 50\,°\mathrm{C}$). A higher cold side temperature would also lead to an increase in the effective permeability. A constant value of 10×10^{-7} kg/m^2-s-Pa is assumed throughout the module as a conservative estimate, in this study. The effect of variations in B is also studied. The channel thickness as well and the gap thickness are set at 1 mm. The feed inlet velocity is about 8.3 cm/s and the heat transfer coefficient within the channel is $h_{\mathrm{f}} = h_{\mathrm{c}} \approx 2400$ W/m^2·K. The channel width is 12 m, and channel length is 6 m, wherever not explicitly stated.

Figure 3 shows the comparison between various MD configurations. All the configurations show a trade-off between permeate flux and GOR, as previously observed for DCMD [27]. Assuming similar capital cost per unit area, a configuration whose performance curve lies towards the top-right is strictly better since it has both higher energy efficiency and flux. At a constant flux, the GOR of CGMD is two times higher than that of PGMD. The energy efficiency of DCMD lies between those of PGMD and CGMD. Similarly, at constant GOR, flux of CGMD is about two times higher than that of PGMD. The reason for this trend in terms of the values of thermal efficiency and effectiveness is shown in Fig. 3b. η decreases with length for all the configurations. The η of AGMD is higher than 0.9 over the entire range of system lengths. The η for PGMD, DCMD and CGMD are lower and decrease more significantly with area. The value of η for these three systems is relatively similar.

One of the important results is that a low thermal conductivity of the gap region, when the gap is filled with water, is not particularly useful in maintaining a higher value of η. This was the motivation behind maintaining low thermal conductivity in the case of PGMD [16] and material gap MD [18]. On the contrary, with a highly conductive gap, as in the case of CGMD, η is only slightly lower. The reason is that η is only a function of the membrane properties and conditions at the boundary of the membrane (Eq. 23). Changes in other parts of the system, can influence η only through changing the boundary conditions across the membrane. An air gap does lead to a higher η at the expense of lower ε. With an increase in length, GOR increases from about 1 to about 15, in spite of the small decrease in η with length. This is a result of the significant increase in ε. DCMD has the largest ε, followed by CGMD, PGMD and AGMD. The higher ε leads to higher overall energy efficiency in the case of CGMD, compared to AGMD and PGMD.

Figure 4 shows the same comparison for a membrane with lower permeability ($B = 5 \times 10^{-7}$kg/m^2-s-Pa). As a consequence of the lower permeability, the η values for all the configurations are lower, although the effect is much more pronounced for CGMD, PGMD and DCMD, where the thermal efficiency drops by

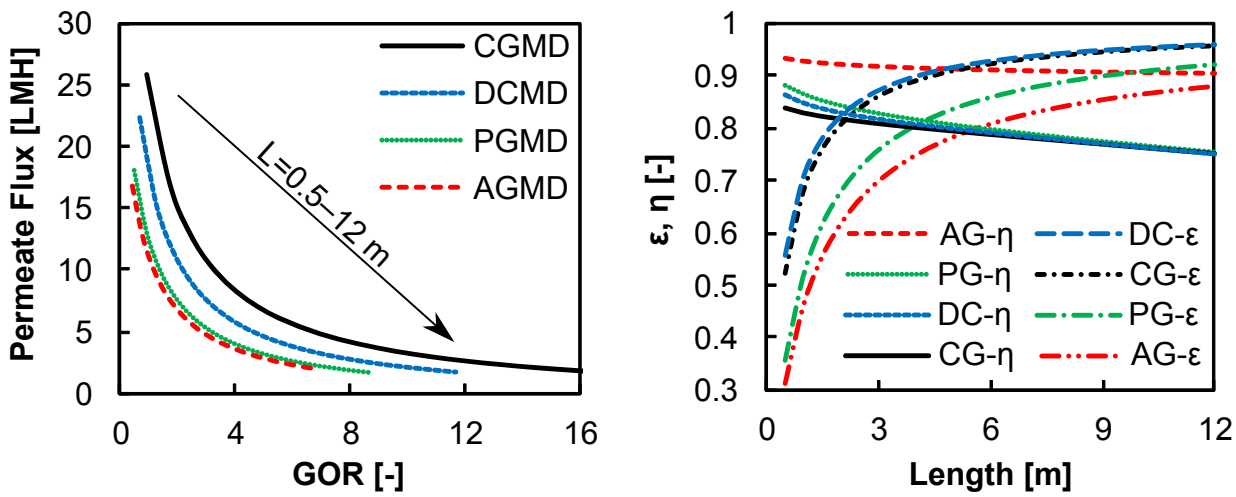

(a) Comparison of flux and GOR.

(b) ε and η variation for various configurations.

Figure 3: Module comparison. $w = 12$ m, $\dot{m}_{\mathrm{f,in}} = 1$ kg/s, $T_{\mathrm{f,in}} = 85\,^{\circ}$C, $T_{\mathrm{c,in}} = 25\,^{\circ}$C, $B = 10 \times 10^{-7}$ kg/m^2-s-Pa, $d_{\mathrm{gap}} = 1$ mm.

0.1 (Fig. 4b). As a result of this, the trends in terms of GOR are also affected. The energy efficiency of CGMD is only 80% higher, compared to 100% higher in the previous case. Also, PGMD which was slightly better than AGMD, becomes worse than AGMD under these conditions. The effect of B on the flux of the various configurations at fixed channel length is shown in Fig. 6b. In AGMD, since the air-gap dominates the resistance to both heat transfer and vapor flux, a change in B does not lead to significant variation in flux or η. Conceptually, Eq. 23 can be used to understand the high η of AGMD by considering the membrane and the air-gap together as a thick "membrane" separating the salt water and pure water interfaces. The overall resistance to heat transfer is largest in AGMD, leading to a low ε and correspondingly higher value of $\mathrm{TTD_{MD}}$. A major portion of this temperature drop happens across the membrane and air gap, occuring between the feed water interface and the condensing film interface at the condensing surface. The overall thermal conductivity of this region is also lower than the effective thermal conductivity of the membrane, leading to a higher value of η.

The relative performance of the various configurations is also affected by the gap thickness. All results are reported for an effective gap thickness of 1 mm. The effective gap thickness is often lower than the thickness of the gap spacer since the membrane gets pressed into the gaps in the spacer and the spacer disrupts the condensation film in AGMD. At very low gap thicknesses, the performance of PGMD overlaps with CGMD. The performance of AGMD improves with decreasing gap thickness, although practically, pure water bridging and flooding can start becoming significant under those conditions pushing AGMD performance closer to that of PGMD at smaller gap thickness.

4. Effect of DCMD external heat exchanger area

Figures 3 and 4 show that the GOR of DCMD is lower than that of CGMD in spite of having both a slightly higher η and ε than CGMD. The reason for the lower overall GOR is the presence of the external heat exchanger (HX) in DCMD for energy recovery.

Equation 7 can be rewritten as follows to enable the comparison with CGMD:

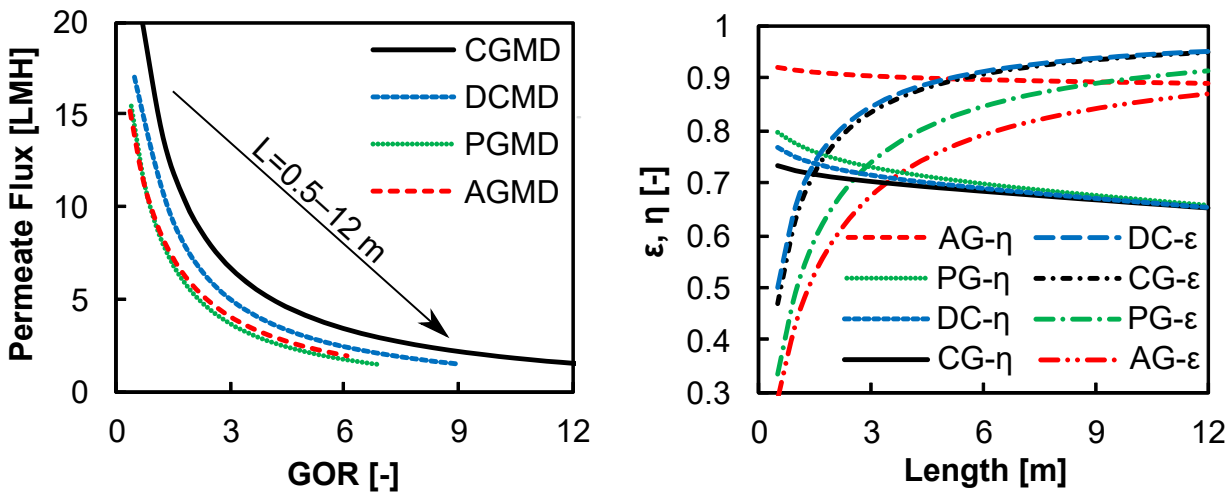

(a) Comparison of MD configurations.

(b) ε and η variation.

Figure 4: Module comparison for lower permeability membrane: $B = 5 \times 10^{-7}$ kg/m^2-s-Pa. $w = 12$ m, $\dot{m}_{\mathrm{f,in}} = 1$ kg/s, $T_{\mathrm{f,in}} = 85\,^{\circ}$C, $T_{\mathrm{c,in}} = 25\,^{\circ}$C, $d_{\mathrm{gap}} = 1$ mm.

$$\begin{aligned}\mathrm{GOR}_{\mathrm{DCMD}} &= \eta \times \frac{\Delta T_{\mathrm{MD}}}{\mathrm{TTD}_{\mathrm{MD}} + \mathrm{TTD}_{\mathrm{HX}}} \\ &= \eta \times \frac{\Delta T_{\mathrm{MD}}}{\mathrm{TTD}_{\mathrm{MD}}} \times \frac{\mathrm{TTD}_{\mathrm{MD}}}{\mathrm{TTD}_{\mathrm{MD}} + \mathrm{TTD}_{\mathrm{HX}}} \\ &= \eta \times \frac{\varepsilon}{1-\varepsilon} \times \frac{\mathrm{TTD}_{\mathrm{MD}}}{\mathrm{TTD}_{\mathrm{MD}} + \mathrm{TTD}_{\mathrm{HX}}} \end{aligned} \tag{15}$$

Note that the mass flow rate of the cold stream varies along the length in DCMD, but ε is still defined as in Eq. 9.

Under similar operating conditions, ε and η are slightly higher for DCMD compared to CGMD (Figs. 3b, 4b) because:

1. DCMD has a lower overall resistance since the gap resistance is eliminated
2. For the same feed inlet flow rate as CGMD, the average flow rate in balanced DCMD is lower. In CGMD the total mass flow rate of the feed and the product in the gap is a constant, whereas the feed flow and pure water flow rates are both maximum at the hot end of the module in DCMD and reduce along the length. For a recovery ratio of 10%, the average feed water flow rate and heat capacity rate are therefore arount 5% lower in DCMD. This leads to a larger NTU, and hence a larger ε.
3. $T_{\mathrm{c,in}}$ is greater than T_0 (ambient temperature, at which feed enters the desalination system (Fig. 1b)) for the DCMD systems considered in this study. This is because the external heat exchanger has a finite TTD and no additional cooling system is used [47]. Flux decreases and energy efficiency increases and with an increase in $T_{\mathrm{c,in}}$.

For an infinite area external HX, $\mathrm{TTD}_{\mathrm{HX}} = 0\,^{\circ}$C, and therefore the GOR of DCMD with an infinite external HX ($\mathrm{GOR}_{\mathrm{DCMD}}^{\infty\mathrm{HX}}$) can be written as:

$$\mathrm{GOR}_{\mathrm{DCMD}}^{\infty\mathrm{HX}} = \eta \times \frac{\varepsilon}{1-\varepsilon} \tag{16}$$

and due to the higher value of ε and η for DCMD compared to a CGMD of the same size, $\mathrm{GOR}_{\mathrm{DCMD}}^{\infty\mathrm{HX}}$ is approximately 5-10% higher than $\mathrm{GOR}_{\mathrm{CGMD}}$.

4.1. Quantifying the loss due to HX: $\mathrm{TTD}_{\mathrm{factor}}$

A new variable, $\mathrm{TTD}_{\mathrm{factor}}$ is introduced to understand the loss associated with using an external HX to recover energy. $\mathrm{TTD}_{\mathrm{factor}} \equiv \frac{\mathrm{TTD}_{\mathrm{MD}}}{\mathrm{TTD}_{\mathrm{MD}}+\mathrm{TTD}_{\mathrm{HX}}}$ is defined as a function of the terminal temperature difference

in the two balanced exchangers, the MD module and external HX. Equation 15 can then be rewritten as:

$$\mathrm{GOR}_{\mathrm{DCMD}} \approx \mathrm{GOR}_{\mathrm{DCMD}}^{\infty\mathrm{HX}} \times \mathrm{TTD}_{\mathrm{factor}} \tag{17}$$

For a DCMD system with additional cooling (Fig. 1b), where the cold water enters the MD module at ambient temperature ($T_{\mathrm{c,in}} = T_0$), the equality in Eq. 17 is exact. For a DCMD system as shown in Fig. 1b, where the cold pure water inlet temperature $T_{\mathrm{c,in}} = T_0 + \mathrm{TTD}_{\mathrm{HX}}$, $\eta \times \frac{\varepsilon}{1-\varepsilon}$ is around 3% higher than $\mathrm{GOR}_{\mathrm{DCMD}}^{\infty\mathrm{HX}}$ when the area of the HX is half that of the membrane, and the deviation decreases as the HX area increases and $T_{\mathrm{c,in}} \to T_0$.

$\mathrm{TTD}_{\mathrm{factor}}$ represents the loss in DCMD associated with having an additional heat exchanger(HX) for energy recovery. If the external HX is as effective as the MD exchanger, and achieves similar TTD as the MD exchanger, $\mathrm{TTD}_{\mathrm{factor}} = 0.5$, leading to DCMD system's GOR being half of $\mathrm{GOR}_{\mathrm{DCMD}}^{\infty\mathrm{HX}}$ and little over half that of a similarly sized CGMD system. If the goal is to transfer heat from fluid A to fluid B, using one HX is always better than using two HXs with an intermediate fluid C that flows between these two HXs (Here fluid C is DCMD's pure water flow loop). The introduction of the intermediate fluid means that the overall heating of fluid B is lower. Only if the second HX is made much larger, the relative loss associated with adding the extra HX and intermediate fluid can be reduced. The idea in the case of DCMD is similar. All the previous results are reported for the case where the area of the external heat exchanger is equal to the area of the membrane, in order to have a fair comparison between systems, since the condenser surface area would be equal to the membrane area in AGMD and PGMD. If CGMD is implemented by adding fins, the effective condenser area would be higher, but if it is implemented by having a very small gap thickness, the condenser area would be equal to the membrane area. The overall heat transfer coefficient for the HX was set at a representative value of $U_{\mathrm{HX}} = 1300$ W/m^2-K, e.g., for a liquid-liquid heat exchanger with copper tubing. Under these conditions, $\mathrm{TTD}_{\mathrm{factor}} = 0.65$, leading to DCMD system's GOR being about 30% lower than that of similarly sized CGMD.

The effect of the external heat exchanger area on $\mathrm{TTD}_{\mathrm{HX}}$ and thereby on $\mathrm{TTD}_{\mathrm{factor}}$ and $\mathrm{GOR}_{\mathrm{DCMD}}$ are shown in Fig. 5. The GOR of DCMD becomes equal to that of similarly sized CGMD system only when the external HX area is seven times that of the membrane area within the MD module. Beyond this area ratio, the GOR of DCMD slightly exceeds that of CGMD. However, an external HX that is seven times larger than the MD module will entail significant increase in the capital expenditure, counterbalancing the energetic improvement.

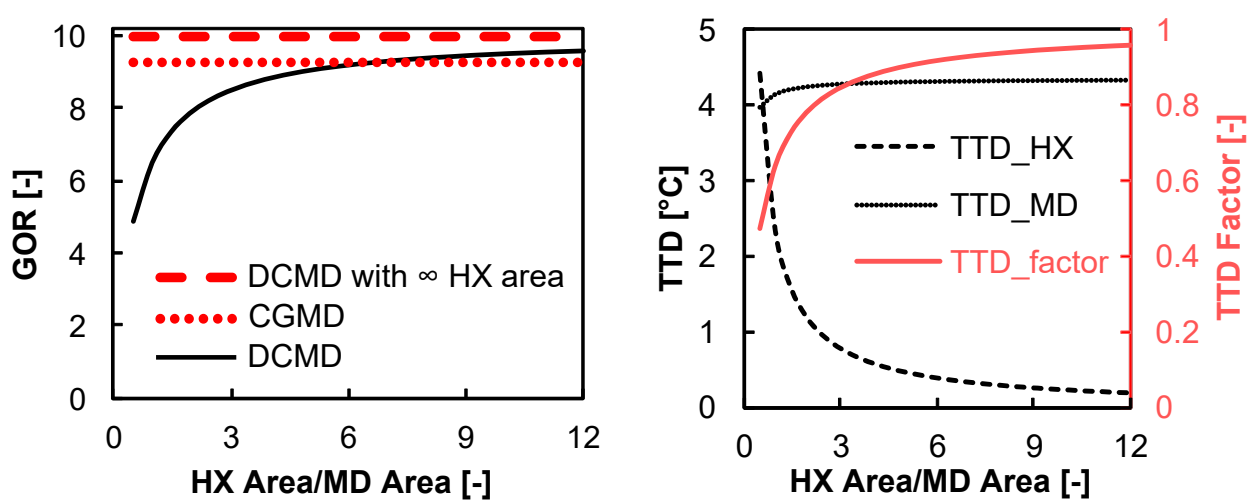

(a) Energy efficiency.

(b) Terminal temperature differences and $\mathrm{TTD}_{\mathrm{factor}}$.

Figure 5: Effect of HX to membrane area ratio on the performance of DCMD. Other parameters are fixed at baseline values specified in Sec. 3.

5. Effect of transport resistances

5.1. Effect of membrane permeability

The influence of membrane permeability (B) on system GOR for various MD configurations is shown in Fig. 6. With the development of novel higher permeability membranes, CGMD and DCMD are set to gain the most, with a two times improvement in GOR associated with an order of magnitude increase in B. The improvement in the case of PGMD is less significant and in the case of AGMD, the improvement with increase in B is even lower. The reason for this is that the membrane constitutes the major resistance in the series of resistances within the MD module, in the case of CGMD and DCMD. On the other hand, in the case of PGMD and AGMD, the gap constitutes the major resistance (Fig. 7), leading to lower improvements with a more permeable membrane. Figure 6b shows the variation in flux with changes in membrane permeability. The increase in flux is more significant for PGMD, CGMD and DCMD compared to the case of AGMD. At lower B, these configurations have significantly lower η as shown in Fig. 4b, and hence lower flux than AGMD. Larger B leads to an increase in η in these systems, leading to higher improvements in flux.

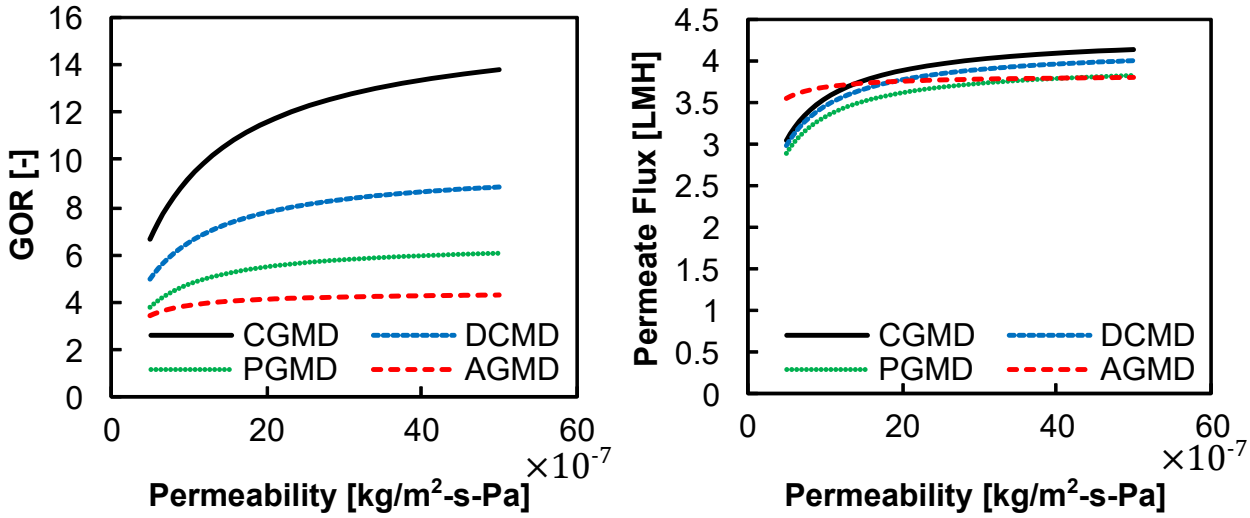

(a) Effect of membrane permeability (B) on GOR.

(b) Effect of membrane permeability (B) on flux.

Figure 6: Effect of pembrane permeability (B). Other parameters are fixed at baseline values specified in Sec. 3.

5.2. Effect of channel heat transfer coefficients

Channel heat transfer is varied by changing the channel depth in the range of 1.5 to 0.5 mm, with higher h at lower channel depth. In CGMD and DCMD, the heat transfer coefficients of the channels contribute significantly to overall resistance (Fig. 7), since the gap resistance itself is negligible. As a result, increasing the feed and cold channel heat transfer coefficient leads to significant improvements in GOR. Since the gap constitutes the major resistance, improvements are once again more modest for AGMD and PGMD, as shown in Fig. 8a. The flux for the various MD configurations is plotted in Fig. 8b. Flux is slightly higher for AGMD over the entire range, due to the higher η in the case of AGMD.

6. Heat exchanger based simplified model of CGMD, PGMD and DCMD

In this section, a simplified heat-exchanger-based mathematical model of MD is developed. Usually MD is modeled by discretization of the module area and solving the transport equations within each computational cell and ensuring mass, momentum and energy balance between the cells [11, 20, 24, 22]. This is computationally expensive and complicated. The ε-NTU method for heat exchangers ([53]) enables evaluation of total heat transfer in a heat exchanger given only the input stream parameters, without discretization of the heat exchanger area.

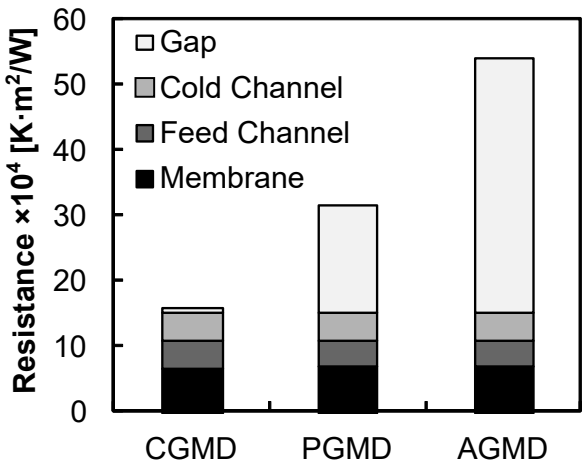

Figure 7: MD module heat transfer resistances. Comparison between modules at baseline conditions specified in Sec. 3.

Inspired by the ε-NTU method, η and ε are rewritten in terms of the transport resistances within the MD system. A single stage membrane distillation module resembles a counter-flow heat exchanger with hot brine and pure product transferring energy into the cooler feed, thereby preheating it (Fig. 1). Similar analogies with heat exchangers have been used to develop simplified effectiveness-MTU (mass transfer units) models for reverse osmosis [54] and pressure retarded osmosis systems [55].

ε of the system can be related to the number of transfer units (NTU) of the module, where NTU is defined as:

$$\mathrm{NTU} = \frac{UA}{\dot{m}c_{\mathrm{p}}} \tag{18}$$

Here, U is the overall heat transfer coefficient of the system in W/m^2-K. The overall heat transfer coefficient has been introduced and used to evaluate DCMD flux multiple times in the literature [36]. Other investigators [24] have used a parameter similar to NTU such as the specific membrane area times a transfer coefficient.

The resistances in permeate and conductive gap MD include boundary layer resistance in the cold and hot streams, the effective resistance of the membrane and the heat conduction resistance of the gap. As a result, the overal heat transfer coefficient U can be expressed as:

$$\frac{1}{U} = \frac{1}{h_{\mathrm{f}}} + \frac{1}{h_{\mathrm{eff,m}}} + \frac{d_{\mathrm{gap}}}{k_{\mathrm{gap}}} + \frac{1}{h_{\mathrm{c}}} \tag{19}$$

where h_{f} is the heat transfer coefficient in the feed, h_{c} is the heat transfer coefficient in the cold channel and $h_{\mathrm{eff,m}}$ is the effective heat transfer coefficient of the membrane.

Across the membrane, both heat and mass transfer occur. The transfer of water vapor through the membrane, which is the fundamental separation step in MD, is driven by a vapor pressure difference. While the other transport resistances are relatively constant along the module length, the heat transfer associated with vapor transport is higher at the higher temperature end due to the exponential nature of vapor pressure dependence on temperature. The total resistance across the membrane $\left(\frac{1}{h_{\mathrm{eff,m}}}\right)$ can be expressed as two resistances in parallel, corresponding to heat conduction $\left(\frac{\delta_{\mathrm{m}}}{k_{\mathrm{m}}}\right)$ and mass transfer $\left(\frac{1}{h_{\mathrm{m}}^{\mathrm{mass}}}\right)$, and so the conductances may be added:

$$h_{\mathrm{eff,m}} = \frac{k_{\mathrm{m}}}{\delta_{\mathrm{m}}} + h_{\mathrm{m}}^{\mathrm{mass}} \tag{20}$$

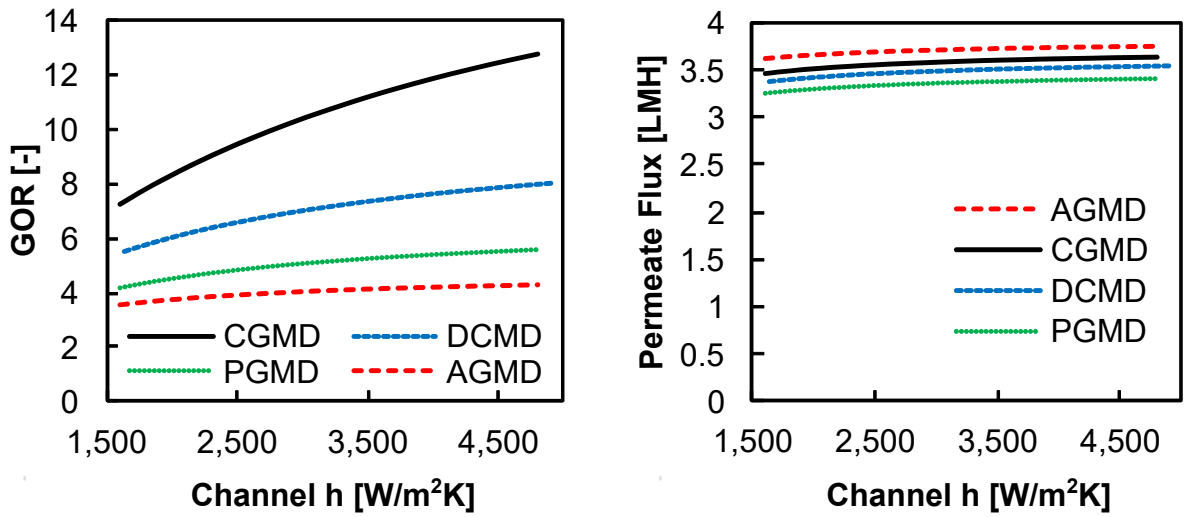

(a) Effect of channel heat transfer coefficients on GOR. (b) Effect of channel heat transfer coefficients on flux.

Figure 8: Effect of channel heat transfer coefficients $h_{\mathrm{f}} = h_{\mathrm{c}}$. h is varied by changing d_{ch} between 0.5–1.5 mm. The feed velocity changes from 4.15 – 12.45 cm/s. Other parameters are fixed at baseline values specified in Sec. 3.

where k_{m} is the effective thermal conductivity of the membrane and is the weighted average of the conductivities of the membrane material (such as PVDF) ($k_{\mathrm{s}} = 0.2$ W/m-K) and the vapor filling the pores ($k_{\mathrm{v}} = 0.02$ W/m-K). This expression is plugged into Eq. 19 to evaluate the overall heat transfer coefficient.

The resistance to mass transfer needs to be rewritten in terms of the temperature difference so that it can be combined with other resistances. A heat transfer coefficient corresponding to vapor transfer across the membrane ($h_{\mathrm{m}}^{\mathrm{mass}}$) is defined such that the following relation between the average vapor pressure difference and average temperature difference across the membrane holds: $Bh_{\mathrm{fg}}\Delta p_{\mathrm{m}} = h_{\mathrm{m}}^{\mathrm{mass}}\Delta T_{\mathrm{m}}$.

The vapor pressure of pure water can be approximately given by $P_{\mathrm{sat}}(T) = A\mathrm{e}^{bT}$ ($A = 1054.8$ Pa, $b = 0.0479$ °C^{-1}. R^2=0.9978 for $T \in [25\,°\mathrm{C}, 85\,°\mathrm{C}]$). On the feed side, water also contains salt, and hence the vapor pressure is given as $p_{\mathrm{f,m}} = P_{\mathrm{sat}}(T_{\mathrm{f,m}}) \times a_{\mathrm{w}}(T_{\mathrm{f,m}}, x_{\mathrm{f,m}}) \approx P_{\mathrm{sat}}(T_{\mathrm{f,m}} - \mathrm{BPE}(T_{\mathrm{f,m}}, x_{\mathrm{f,m}}))$. At any local position in the module:

$$\begin{aligned} h_{\mathrm{m}}^{\mathrm{mass}} &= Bh_{\mathrm{fg}}\frac{\Delta p_{\mathrm{m}}}{\Delta T_{\mathrm{m}}} \\ &= Bh_{\mathrm{fg}}\frac{\left(A\mathrm{e}^{b(T_{\mathrm{p,m}}+\Delta T_{\mathrm{m}}-\mathrm{BPE}_{\mathrm{f,m}})} - A\mathrm{e}^{bT_{\mathrm{p,m}}}\right)}{\Delta T_{\mathrm{m}}} \\ &= Bh_{\mathrm{fg}}bA\mathrm{e}^{bT_{\mathrm{p,m}}}\left(1 - \frac{\mathrm{BPE}}{\Delta T_{\mathrm{m}}}\right)\left(\frac{\mathrm{e}^{b(\Delta T_{\mathrm{m}}-\mathrm{BPE})} - 1}{b\left(\Delta T_{\mathrm{m}} - \mathrm{BPE}\right)}\right) \end{aligned} \tag{21}$$

Note that this equation is not applicable to AGMD since pure water is not in contact with the cold side of the membrane in AGMD.

Equation 21 shows that the resistance of the membrane to mass transfer is lower at higher temperatures. This is a direct result of the exponential nature of the vapor pressure dependence on temperature. In addition to this, B itself is in reality temperature dependent, and is higher at higher temperatures, further reducing mass transfer resistance at the hot end of the module. These effects are simplified by defining an average mass transfer resistance of the membrane as a function of some average value of $T_{\mathrm{p,m}}$, denoted by T_{avg} and by defining an average value of BPE at the feed membrane interface within the module.

ε can then be evaluated ([53]) assuming a perfect counter-flow heat exchanger as

$$\varepsilon = \frac{\mathrm{NTU}}{1 + \mathrm{NTU}} \tag{22}$$

η can be evaluated as the fraction of the heat transferred through the mass transfer resistance (Eq. 20) as

$$\begin{aligned}\eta &= \frac{Bh_{\mathrm{fg}}\Delta p_{\mathrm{m}}}{Bh_{\mathrm{fg}}\Delta p_{\mathrm{m}} + \frac{k_{\mathrm{m}}\Delta T_{\mathrm{m}}}{\delta_{\mathrm{m}}}} \\ &= \frac{1}{1 + \frac{k_{\mathrm{m}}}{\delta_{\mathrm{m}} B h_{\mathrm{fg}}}\frac{\Delta T_{\mathrm{m}}}{\Delta p_{\mathrm{m}}}} \\ &= \frac{1}{1 + \frac{k_{\mathrm{m}}}{\delta_{\mathrm{m}}}\frac{1}{h_{\mathrm{m}}^{\mathrm{mass}}}}\end{aligned} \tag{23}$$

The ratio of heat to mass conductance $\left(\frac{k_{\mathrm{m}}}{\delta_{\mathrm{m}} B}\right)$ is important [42]. A lower value of this fraction leads to a higher η. Therefore, the thermal efficiency is very sensitive to this parameter. Additionally, a higher temperature on the hot or cold side would lead to a higher η as has been reported by most researchers in the past. Finally, a larger feed salinity leading to higher BPE results in a lower value of η. Under this condition, it is important to keep ΔT_{m} much larger than BPE. This is the reason why Eykens et al. [43] found that at higher feed salinities in the DCMD configuration, thicker membranes with lower transfer coefficient have better thermal performance.

The average temperature difference across the membrane, ΔT_{m}, is an unknown in Eqs. 23, 21. It can be related to the TTD of the MD system, as a function of the heat transfer resistance offered by the membrane $\left(\frac{1}{h_{\mathrm{eff,m}}}\right)$ and the overall resistance $\left(\frac{1}{U}\right)$ as:

$$\frac{\mathrm{TTD}}{((1/U))} = \frac{\Delta T_{\mathrm{m}}}{1/h_{\mathrm{eff,m}}} \tag{24}$$

where, TTD itself is a function of ε and the exchanger top and bottom temperatures:

$$\mathrm{TTD} = (1-\varepsilon)\cdot(T_{\mathrm{f,in}} - T_{\mathrm{c,in}}) \tag{25}$$

and hence, these equations are solved iteratively.

Equations 22 and 23 can be substituted into Eq. 10 to evaluate GOR. Additionally, heat transfer rate into the system can be expressed as a function of the system top and bottom temperatures and ε:

$$\dot{Q}_{\mathrm{h}} = \dot{m}_{\mathrm{f,in}} c_{\mathrm{p}} \times (1-\varepsilon)\,(T_{\mathrm{f,in}} - T_{\mathrm{c,in}}) \tag{26}$$

and flux can be evaluated by substituting values of $\dot{Q}_{\mathrm{h}}$ and GOR into Eqs. 1 and 2.

A fit for T_{avg} as a function of top temperature is obtained from the detailed finite difference numerical model as $T_{\mathrm{avg}} = (0.3586 \times T_{\mathrm{f,in}} + 21.922)$. The average BPE at the membrane interface for the case of seawater salinity considered in this study is set at 0.4 °C. The entire set of 33 equations that were solved with Engineering Equation Solver [56] for the simplified HX based model of PGMD and CGMD is provided in Appendix A.2.

The equations for modeling DCMD with an external heat exchanger (based on additional equations discussed in Section 4) are also provided in Appendix A.2.

6.1. Validation of the proposed simplified model

The proposed heat-exchanger-based energy efficiency evaluation model is compared against the more detailed finite difference numerical model over a range of top temperatures ($T_{\mathrm{f,in}}$ = 40–85°C) and module areas (L = 0.5–12 m). Additionally comparisons are carried out at fixed L = 6 m and $T_{\mathrm{f,in}}$ = 85 °C, by varying the membrane permeability (B = 5–50 $\times 10^{-7}$ kg/m^2-s-Pa), channel heat transfer coefficients ($h_{\mathrm{f}} = h_{\mathrm{c}}$ = 1600–4800 W/m^2-K) and gap conductivity (k_{m} = 0.6–30 W/m-K). h_{fg} is evaluated at T = 25 °C. The differences in the simplified model results compared to the discretized model, as a percent deviation in flux and GOR are plotted in Fig. 9. The deviation tends to increase at lower feed inlet temperature and shorter module length, and the maximum deviation is about 11%. The deviations in the case of DCMD are shown in Fig. A.12, and are also lower than 10%.

The finite difference model with 100 computational cells has over 2000 equations and takes about 6 seconds for each computation, whereas the heat exchanger based model is evaluated in about 1 μs.

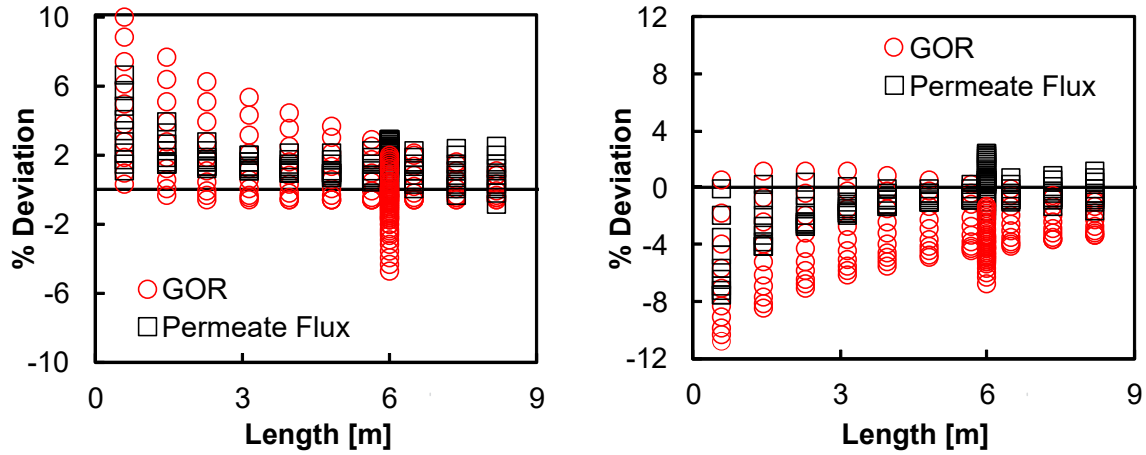

(a) Comparison of simplified HX based model and finite difference model of CGMD. $L = 0.6$–8.2m and $T_{\mathrm{f,in}} = 40$–$85\,^{\circ}$C. $B = 5 \times 10^{-7}$–50×10^{7} kg/m^2-s-Pa. $h_{\mathrm{f}} = 1600$–4800 W/m^2-K. $k_{\mathrm{gap}} = 0.6$–30 W/m-K. Other parameters are held constant at baseline values specified in Sec. 3.

(b) Comparison of simplified HX based model and finite difference model of PGMD. $k_{\mathrm{gap}} = 0.6$ W/m·K. $L = 0.6$–8.2m and $T_{\mathrm{f,in}} = 40$–$85\,^{\circ}$C. $B = 5 \times 10^{-7}$–50×10^{7} kg/m^2-s-Pa. $h_{\mathrm{f}} = 1600$–4800 W/m^2-K. Other parameters are held constant at baseline values specified in Sec. 3.

Figure 9: Percentage deviation in GOR and flux evaluated by heat exchanger based model compared to finite difference 1-D model over a wide range of operating conditions.

7. Conclusions

Balanced single-stage MD systems can be approximated and analyzed as counter-flow heat exchangers. The exchanger effectiveness ε and NTU are key parameters along with η to understand the energetic performance of these systems. Using this framework, insights on the relative performance of various MD configurations as well as a simplified model are developed.

1. Energy efficiency of MD systems with internal heat regeneration is expressed in terms of thermal efficiency (η) and exchanger effectiveness (ε) as $\mathrm{GOR} = \eta \frac{\varepsilon}{1-\varepsilon}$. This expression is useful to understand the higher effect of the heat energy recovery (ε) compared to reducing heat conduction losses (η). Design of MD module should focus on increasing overall U, while the design of the membranes should focus on maximizing η.
2. An expression for the theoretical maximum GOR for single-stage MD is derived as a function of temperatures and feed salinity or boiling point elevation (BPE) as: $\mathrm{GOR}_{\mathrm{limit,MD}} = \frac{T_{\mathrm{f,in}} - T_{\mathrm{c,in}}}{\mathrm{BPE}_{\mathrm{f,in}}} - 1$, for an ideal perfectly insulating membrane using the proposed model. This expression is validated against the thermodynamic limit for GOR evaluated for a generic thermal desalination system with no entropy generation.
3. The GOR of DCMD can be expressed as $\mathrm{GOR}_{\mathrm{DCMD}}^{\infty\mathrm{HX}} \times \mathrm{TTD}_{\mathrm{factor}}$, where $\mathrm{GOR}_{\mathrm{DCMD}}^{\infty\mathrm{HX}}$ corresponds to the energy efficiency when the external heat exchanger area is infinite, and $\mathrm{TTD}_{\mathrm{factor}}$ quantifies the loss associated with having finite external HX area. While $\mathrm{GOR}_{\mathrm{DCMD}}^{\infty\mathrm{HX}}$ is around 5–10% higher than that of a similarly sized CGMD system, the actual GOR of DCMD is equal to that of that of a similar size CGMD system only when the external heat exchanger area is about 7 times higher than the membrane area.
4. At a constant value of flux (J) and area of condensing surface, GOR of CGMD is higher than that of DCMD and PGMD. CGMD represents the practical upper limit performance of both PGMD and DCMD. A PGMD system with very low gap thickness and a DCMD system with large external HX area compared to membrane area approach this limit. Membrane and flow channel heat transfer resistances are significant in the case of DCMD and CGMD, whereas the gap constitutes the major heat transfer resistance in the case of AGMD and PGMD. At seawater salinity, and for the membrane properties and conditions considered in this study, the GOR of AGMD is approximately equal to that of PGMD.

5. ε is expressed as a function of NTU through an analogy with counter-flow heat exchangers. GOR can therefore be expressed as $\eta \times$ NTU for AGMD, PGMD and DCMD. η is also approximated as a function of the membrane properties and temperatures across the membrane for PG, CG and DCMD. A simplified model for predicting the performance of these MD systems without detailed modeling is presented.
6. The percent deviation associated with using the simplified heat-exchanger parameter model for predicting GOR and flux of CGMD, PGMD and DCMD is below 11% over a wide range of operating conditions.

Acknowledgments

This work was funded by the Cooperative Agreement Between the Masdar Institute of Science and Technology (Masdar Institute), Abu Dhabi, UAE and the Massachusetts Institute of Technology (MIT), Cambridge, MA, USA, Reference No. 02/MI/MI/CP/11/07633/GEN/G/00, and facilitated by the MIT Deshpande Center for Technological Innovation and the Masdar Institute Center for Innovation and Entrepreneurship (iInnovation).

The authors acknowledge Tamanna Urmi for help with proofreading the manuscript.

Appendix A. Appendix

Appendix A.1. Model validation

The MD system is discretized along the length direction and in each computational cell, the water flux and total heat flux across the membrane are evaluated. The transport model across the membrane was validated using experimental results from a bench-top apparatus [20, 57]. Using the mass and heat flux evaluated, properties at subsequent cells are evaluated by applying conservation of mass, species and energy. Experimental and numerical modeling results are provided in Winter [58] for systems with larger membrane area of around 10 m^2.

Figure A.10 compares the current model predictions with Winter's model (which was validated against experimental data) for AGMD, PGMD and DCMD systems with variation of feed inlet temperature and feed inlet flow rate. The following inputs were used in the present model for comparison: $T_{\mathrm{f,in}} = 80\,^{\circ}\mathrm{C}$, $T_{\mathrm{c,in}} = 25\,^{\circ}\mathrm{C}$, $s_{\mathrm{f,in}} = 0.2$ g/kg, $\delta_{\mathrm{m}} = 70$ μm, $k_{\mathrm{m}} = 0.25$ W/m-K, $L = 10$ m (6.5 m for the AGMD module), $w = 0.7$ m, $d_{\mathrm{ch}} = 1.6$ mm (1 mm for the AGMD module, corresponding to half of the reported channel height). The effective gap thickness was set at around 65% of the design value for AGMD ($d_{\mathrm{gap}} = 1.3$ mm) based on experience with bench-scale apparatus experiments where the membrane gets pushed into the gaps in the spacer. The gap thickness for PGMD is 0.5 mm and the effective thermal conductivity of the gap is set as 0.5 W/m-K. The membrane permeability was set at a constant value of $B = 9 \times 10^{-7}$ kg/m^2-s-Pa for all the simulations. The DCMD system is balanced.

The correct trends are captured by the present model for all three configurations. The effects of spiral wound module geometry, spacer design and other details have not been incorporated in detail in the model, and would be necessary to make more accurate predictions for specific systems. This work focuses on comparing various MD configurations that employ the same membrane and have similar geometry. In this context, it is noteworthy that the present model predicts similar trends as those observed by Winter, for the cross-over in performance between the PGMD and DCMD. For DCMD systems, an external heat exchanger with fixed TTD of 2 °C was used to model the HX, and additional permeate cooling was assumed so that the pure water inlet temperature into the MD module is equal to 25 °C. At low feed inlet temperature and feed flow rate, PGMD outperforms DCMD. The TTD of the MD module decreases under these conditions, whereas the external HX TTD is fixed, thereby limiting the energy efficiency of the overall system. The effect of the external HX area and TTD on DCMD GOR is discussed in Section 4.

Figure A.11 shows that the present model predicts similar trends in terms of the effect of the gap thickness in PGMD as the discretization model and experimental results reported by Winter. A PGMD system with a vanishingly small gap is one realization of CGMD, and hence the performance prediction for CGMD is also similar between the two models.

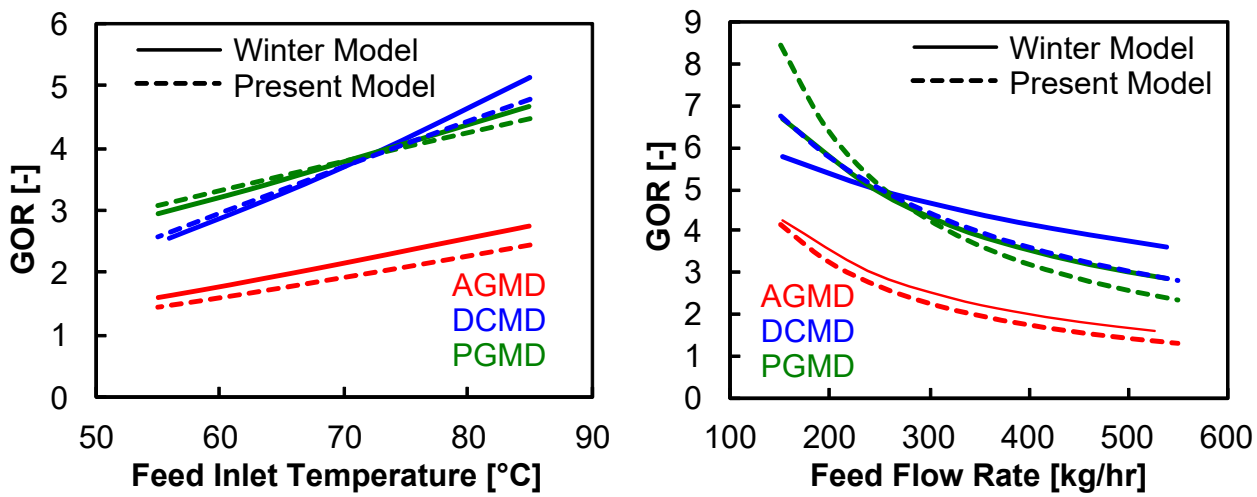

(a) GOR of AGMD, PGMD and DCMD as a function of feed inlet temperature. $\dot{m}_{\mathrm{f}} = 300$ kg/hr.

(b) GOR of AGMD, PGMD and DCMD as a function of feed flow rate.

Figure A.10: Comparison of present model with results from Winter [58] for large spiral-wound MD modules.

Appendix A.2. EES Equations for simplified model of PGMD, CGMD and DCMD

Heat transfer coefficients in the channels

$$h_{\mathrm{t,f}} = 2400 \ \left[\mathrm{W/m^2{\cdot}K}\right] \tag{A.1}$$

$$h_{\mathrm{t,c}} = h_{\mathrm{t,f}} \tag{A.2}$$

Temperatures

$$T_{\mathrm{top}} = 85 \ \left[\mathrm{C}\right] \tag{A.3}$$

$$T_{\mathrm{bottom}} = 25 \ \left[\mathrm{C}\right] \tag{A.4}$$

Geometry

$$L = 6 \ \left[\mathrm{m}\right] \tag{A.5}$$

$$w = 12 \ \left[\mathrm{m}\right] \tag{A.6}$$

$$A = w \cdot L \tag{A.7}$$

Membrane characteristics

$$B = 10 \times 10^{-7} \ \left[\mathrm{kg/m^2{\cdot}s{\cdot}Pa}\right] \tag{A.8}$$

$$K_{\mathrm{cond}} = \left(\frac{k_{\mathrm{m}}}{\delta_{\mathrm{m}}}\right) = 307.83 \ \left[\mathrm{W/m^2{\cdot}K}\right] \tag{A.9}$$

Flow rates

$$\dot{m}_{\mathrm{f,in}} = 1 \ \left[\mathrm{kg/s}\right] \tag{A.10}$$

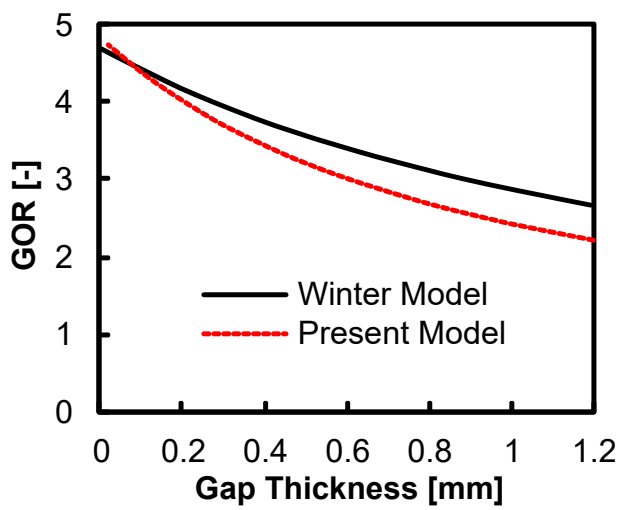

Figure A.11: Comparison of present model with results from Winter [58] on the effect of gap thickness in PGMD. $\dot{m}_{\mathrm{f}}$ =400 kg/hr.

$$c_{\mathrm{p,f}} = 4000 \ \ [\mathrm{J/kg \cdot C}] \tag{A.11}$$

$$\dot{C}_1 = \dot{m}_{\mathrm{f,in}} \cdot c_{\mathrm{p,f}} \tag{A.12}$$

$$\dot{C}_2 = \dot{C}_1 \tag{A.13}$$

Gap

$$k_{\mathrm{gap}} = 0.6\,(\mathrm{PGMD})\ \mathrm{or}\ 10\,(\mathrm{CGMD})\ \mathrm{or}\ 100000\,(\mathrm{DCMD}) \ \ [\mathrm{W/m \cdot K}] \tag{A.14}$$

$$d_{\mathrm{gap}} = 0.001 \ \ [\mathrm{m}] \tag{A.15}$$

Salinity effect

$$\mathrm{BPE} = 0.4 \ \ [\mathrm{C}] \tag{A.16}$$

$$T_{\mathrm{p,avg}} = (0.3586 \cdot T_{\mathrm{top}} + 21.922) \tag{A.17}$$

Membrane transfer coefficient. A and b are fitting parameters for exponential fit of $p_{\mathrm{vap}} = Ae^{\mathrm{b} \cdot T}$, where T is in °C.

$$b = 0.0479 \tag{A.18}$$

$$A = 1054.8 \tag{A.19}$$

$$\mathrm{MT_{coeff}} = b \cdot A \cdot \exp\left(b \cdot T_{\mathrm{p,avg}}\right) \cdot \left(1 - \frac{\mathrm{BPE}}{\Delta T_{\mathrm{m}}}\right) \cdot \left(\frac{\exp\left(b \cdot (\Delta T_{\mathrm{m}} - \mathrm{BPE})\right) - 1}{b \cdot (\Delta T_{\mathrm{m}} - \mathrm{BPE})}\right) \tag{A.20}$$

Parallel conductances through the mass transfer route and the heat transfer throught he membrane

$$h_{\mathrm{eff,m}} = \mathrm{MT_{coeff}} \cdot B \cdot h_{\mathrm{fg}} + K_{\mathrm{cond}} \tag{A.21}$$

Overall Transfer Coefficient

$$\frac{1}{U} = \frac{1}{h_{\mathrm{t,f}}} + \frac{1}{h_{\mathrm{eff,m}}} + \frac{1}{h_{\mathrm{t,c}}} + \frac{d_{\mathrm{gap}}}{k_{\mathrm{gap}}} \tag{A.22}$$

ΔT_m as a function of overall TTD

$$\frac{\mathrm{TTD}}{((1/U))} = \frac{\Delta T_{\mathrm{m}}}{1/h_{\mathrm{eff,m}}} \tag{A.23}$$

$$h_{\mathrm{fg}} = 2.442 \times 10^6 \ \ [\mathrm{J/kg}] \tag{A.24}$$

NTU - ε relationship

$$\mathrm{NTU} = \frac{U \cdot A}{\dot{C}_1} \tag{A.25}$$

$$\varepsilon = \mathrm{HX}\Big(\text{‘counterflow’ }, \ \mathrm{NTU}, \ \dot{C}_1, \ \dot{C}_2, \ \text{‘epsilon’ }\Big) \tag{A.26}$$

Outputs

$$\mathrm{TTD} = (1 - \varepsilon) \cdot \Delta T_{\mathrm{total}} \tag{A.27}$$

$$\eta = \frac{1}{1 + \left(\left(\frac{K_{\mathrm{cond}}}{B \cdot h_{\mathrm{fg}}}\right) \cdot \left(\frac{1}{\mathrm{MT_{coeff}}}\right)\right)} \tag{A.28}$$

$$\dot{m}_{\mathrm{p}} = \frac{\mathrm{GOR} \cdot Q_{\mathrm{in}}}{h_{\mathrm{fg}}} \tag{A.29}$$

$$J = \frac{\dot{m}_{\mathrm{p}} \cdot 3600}{A} \tag{A.30}$$

Case 1. CGMD and PGMD

$$\mathrm{GOR} = \eta \cdot \frac{\varepsilon}{1 - \varepsilon} \tag{A.31}$$

$$Q_{\mathrm{in}} = \dot{C}_1 \cdot \mathrm{TTD} \tag{A.32}$$

$$\Delta T_{\mathrm{total}} = T_{\mathrm{top}} - T_{\mathrm{bottom}} \tag{A.33}$$

Case 2. DCMD

$$\mathrm{GOR} = \eta \cdot \frac{\varepsilon}{1 - \varepsilon} \cdot \mathrm{TTD_{factor}} \tag{A.34}$$

$$Q_{\mathrm{in}} = \dot{C}_1 \cdot (\mathrm{TTD} + \mathrm{TTD_{HX}}) \tag{A.35}$$

$$\Delta T_{\mathrm{total}} = T_{\mathrm{top}} - T_{\mathrm{bottom,MD}} \tag{A.36}$$

$$\mathrm{TTD}_{\mathrm{factor}} = \frac{\mathrm{TTD}}{\mathrm{TTD} + \mathrm{TTD}_{\mathrm{HX}}} \tag{A.37}$$

External Heat Exchanger

$$A_{\mathrm{HX}} = A \tag{A.38}$$

$$U_{\mathrm{HX}} = 1300 \ \left[\mathrm{W/m^2{\cdot}K}\right] \tag{A.39}$$

$$\mathrm{NTU}_{\mathrm{HX}} = \frac{U_{\mathrm{HX}} \cdot A_{\mathrm{HX}}}{\dot{C}_1} \tag{A.40}$$

$$\varepsilon_{\mathrm{HX}} = HX\left(\text{'counterflow'}\ ,\ \mathrm{NTU}_{\mathrm{HX}},\ \dot{C}_1,\ \dot{C}_2,\ \text{'epsilon'}\ \right) \tag{A.41}$$

$$\mathrm{TTD}_{\mathrm{HX}} = (1 - \varepsilon_{\mathrm{HX}}) \cdot \Delta T_{\mathrm{total,HX}} \tag{A.42}$$

$$\Delta T_{\mathrm{total,HX}} = T_{\mathrm{top}} - \mathrm{TTD} - T_{\mathrm{bottom}} \tag{A.43}$$

$$T_{\mathrm{bottom,MD}} = T_{\mathrm{bottom}} + \mathrm{TTD}_{\mathrm{HX}} \tag{A.44}$$

The difference between the HX based model and the finite difference model for DCMD are shown in Fig. A.12. The maximum deviation between the two models is lesser than 10% in this case as well.

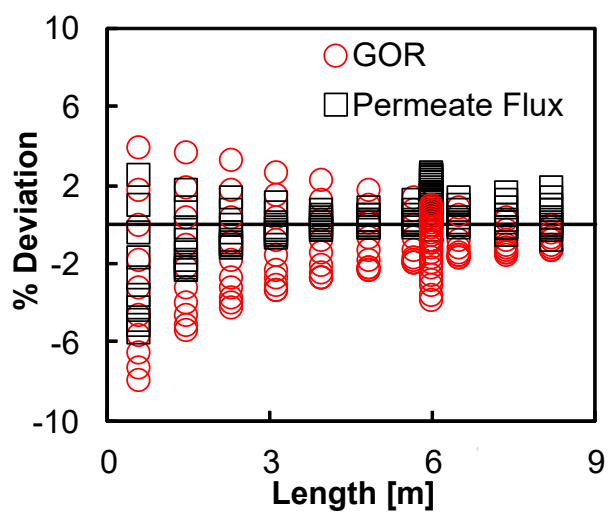

Figure A.12: Comparison of simplified HX based model and finite difference model of DCMD over a wide range of operating conditions. L = 0.6–8.2m and $T_{\mathrm{f,in}}$ = 40–85 °C. $B = 5 \times 10^{-7}$–50×10^{7} kg/m^2-s-Pa. h_{f} = 1600–4800 W/m^2-K. Other parameters are held constant at baseline values specified in Sec. 3.

References

[1] T. Pankratz, IDA Desalination Yearbook 2015–2016, Media Analytics Ltc, Oxford, UK, 2015, International Desalination Association, Global Water Intelligence, and DesalData.
URL https://www.globalwaterintel.com/market-intelligence-reports/ida-desalination-yearbook-2015-2016

[2] N. Ghaffour, S. Lattemann, T. Missimer, K. C. Ng, S. Sinha, G. Amy, Renewable energy-driven innovative energy-efficient desalination technologies, Applied Energy 136 (2014) 1155–1165. doi:10.1016/j.apenergy.2014.03.033.
URL http://www.sciencedirect.com/science/article/pii/S0306261914002633

[3] R. Sarbatly, C.-K. Chiam, Evaluation of geothermal energy in desalination by vacuum membrane distillation, Applied Energy 112 (2013) 737–746. doi:10.1016/j.apenergy.2012.12.028.
URL http://www.sciencedirect.com/science/article/pii/S0306261912009105

[4] F. Suarez, J. A. Ruskowitz, S. W. Tyler, A. E. Childress, Renewable water: Direct contact membrane distillation coupled with solar ponds, Applied Energy 158 (2015) 532–539. doi:10.1016/j.apenergy.2015.08.110.
URL http://www.sciencedirect.com/science/article/pii/S0306261915010466

[5] G. Zaragoza, A. Ruiz-Aguirre, E. Guillén-Burrieza, Efficiency in the use of solar thermal energy of small membrane desalination systems for decentralized water production, Applied Energy 130 (2014) 491–499. doi:10.1016/j.apenergy.2014.02.024.
URL http://www.sciencedirect.com/science/article/pii/S0306261914001603

[6] L. M. Camacho, L. Dumée, J. Zhang, J.-d. Li, M. Duke, J. Gomez, S. Gray, et al., Advances in membrane distillation for water desalination and purification applications, Water 5 (1) (2013) 94–196. doi:10.3390/w5010094.
URL http://www.mdpi.com/2073-4441/5/1/94/

[7] R. B. Saffarini, E. K. Summers, H. A. Arafat, J. H. Lienhard V, Economic evaluation of stand-alone solar powered membrane distillation systems, Desalination 299 (2012) 55–62. doi:10.1016/j.desal.2012.05.017.
URL http://www.sciencedirect.com/science/article/pii/S0011916412002779

[8] M. Khayet, T. Matsuura, Membrane Distillation Principles and Applications, Elsevier, 2011.

[9] D. E. M. Warsinger, J. Swaminathan, J. H. Lienhard V, Effect of module inclination angle on air gap membrane distillation, in: Proceedings of the 15th International Heat Transfer Conference, IHTC-15, Paper No. IHTC15-9351, Kyoto, Japan August 2014.
URL http://web.mit.edu/lienhard/www/papers/conf/IHTC15-9351_Warsinger.pdf

[10] D. M. Warsinger, J. Swaminathan, L. Maswadeh, J. H. Lienhard V, Superhydrophobic condenser surfaces for air gap membrane distillation, Journal of Membrane Science 492 (2015) 578–587.

[11] E. K. Summers, H. A. Arafat, J. H. Lienhard V, Energy efficiency comparison of single-stage membrane distillation (MD) desalination cycles in different configurations, Desalination 290 (2012) 54–66. doi:10.1016/j.desal.2012.01.004.
URL http://linkinghub.elsevier.com/retrieve/pii/S0011916412000264

[12] M. I. Hassan, A. T. Brimmo, J. Swaminathan, J. H. Lienhard V, H. A. Arafat, A new vacuum membrane distillation system using an aspirator: Concept modelling and optimization, Desalination and Water Treatment 57 (2016) 12915—12928. doi:10.1080/19443994.2015.1060902.
URL http://www.tandfonline.com/doi/abs/10.1080/19443994.2015.1060902?journalCode=tdwt20#.VaCPydgtFZQ

[13] H. W. Chung, J. Swaminathan, D. M. Warsinger, J. H. Lienhard V, Multistage vacuum membrane distillation (MSVMD) systems for high salinity applications, Journal of Membrane Science 497 (2016) 128–141. doi:10.1016/j.memsci.2015.09.009.
URL http://www.sciencedirect.com/science/article/pii/S0376738815301733

[14] E. Summers, J. H. Lienhard V, Cycle performance of multi-stage vacuum membrane distillation (MS-VMD) systems, in: Proceedings of the 2013 IDA World Congress on Desalination and Water Reuse, Tianjin, China, 2013.
URL http://web.mit.edu/lienhard/www/papers/conf/SUMMERS_IDA_Tianjin_2013.pdf

[15] J. Swaminathan, J. H. Lienhard V, Energy efficiency of sweeping gas membrane distillation desalination cycles, in: Proceedings of the 22nd National and 11th International ISHMT-ASME Heat and Mass Transfer Conference, IIT Kharagpur, India, 2013.
URL http://web.mit.edu/lienhard/www/papers/conf/SWAMINATHAN_ISHMT_2013.pdf

[16] D. Winter, J. Koschikowski, M. Wieghaus, Desalination using membrane distillation: Experimental studies on full scale spiral wound modules, Journal of Membrane Science 375 (1-2) (2011) 104–112. doi:10.1016/j.memsci.2011.03.030.
URL http://linkinghub.elsevier.com/retrieve/pii/S0376738811002067

[17] A. Cipollina, M. Di Sparti, A. Tamburini, G. Micale, Development of a Membrane Distillation module for solar energy seawater desalination, Chemical Engineering Research and Design 90 (12) (2012) 2101–2121. doi:10.1016/j.cherd.2012.05.021.
URL http://linkinghub.elsevier.com/retrieve/pii/S0263876212002444

[18] L. Francis, N. Ghaffour, A. A. Alsaadi, G. L. Amy, Material gap membrane distillation: A new design for water vapor flux enhancement, Journal of Membrane Science 448 (2013) 240–247. doi:10.1016/j.memsci.2013.08.013.
URL http://www.sciencedirect.com/science/article/pii/S0376738813006595

[19] Z. Ma, T. D. Davis, J. R. Irish, G. D. Winch, Membrane distillation system and method, US Patent App. 12/694,757 (Jan. 27 2010).

[20] J. Swaminathan, H. W. Chung, D. Warsinger, F. Al-Marzooqi, H. A. Arafat, J. H. Lienhard V, Energy efficiency of permeate gap and novel conductive gap membrane distillation, Journal of Membrane Science 502 (2016) 171–178. doi:10.1016/j.memsci.2015.12.017.
URL http://www.sciencedirect.com/science/article/pii/S0376738815303616

[21] E. K. Summers, J. H. Lienhard V, Experimental study of thermal performance in air gap membrane distillation systems including direct solar heating of membranes, Desalination 330 (2013) 100–111. doi:10.1016/j.desal.2013.09.023.
URL http://www.sciencedirect.com/science/article/pii/S0011916413004554

[22] G. Zuo, R. Wang, R. Field, A. G. Fane, Energy efficiency evaluation and economic analyses of direct contact membrane distillation system using Aspen Plus, Desalination 283 (2011) 237–244. doi:10.1016/j.desal.2011.04.048.
URL http://linkinghub.elsevier.com/retrieve/pii/S0011916411003869

[23] J. Gilron, L. Song, K. K. Sirkar, Design for cascade of crossflow direct contact membrane distillation, Industrial & Engineering Chemistry Research 46 (8) (2007) 2324–2334. doi:10.1021/ie060999k.
URL http://pubs.acs.org/doi/abs/10.1021/ie060999k

[24] S. Lin, N. Y. Yip, M. Elimelech, Direct contact membrane distillation with heat recovery: Thermodynamic insights from module scale modeling, Journal of Membrane Science 453 (2014) 498–515. doi:10.1016/j.memsci.2013.11.016.
URL http://www.sciencedirect.com/science/article/pii/S0376738813009010

[25] Q. He, P. Li, H. Geng, C. Zhang, J. Wang, H. Chang, Modeling and optimization of air gap membrane distillation system for desalination, Desalination 354 (2014) 68–75. doi:10.1016/j.desal.2014.09.022.
URL http://linkinghub.elsevier.com/retrieve/pii/S0011916414004974

[26] H. Geng, H. Wu, P. Li, Q. He, Study on a new air-gap membrane distillation module for desalination, Desalination 334 (1) (2014) 29–38. doi:10.1016/j.desal.2013.11.037.
URL http://www.sciencedirect.com/science/article/pii/S0011916413005626

[27] G. Guan, X. Yang, R. Wang, A. G. Fane, Evaluation of heat utilization in membrane distillation desalination system integrated with heat recovery, Desalination 366 (2015) 80–93. doi:10.1016/j.desal.2015.01.013.
URL http://linkinghub.elsevier.com/retrieve/pii/S0011916415000181

[28] R. Tian, H. Gao, X. Yang, S. Yan, S. Li, A new enhancement technique on air gap membrane distillation, Desalination 332 (1) (2014) 52–59. doi:10.1016/j.desal.2013.10.016.
URL https://www.engineeringvillage.com/blog/document.url?mid=cpx_172b3a9114cc37805cbM76d810178163171&database=cpx

[29] H. Y. Wu, M. Tay, R. W. Field, Novel method for the design and assessment of direct contact membrane distillation modules, Journal of Membrane Science 513 (2016) 260–269. doi:10.1016/j.memsci.2016.04.009.
URL http://www.sciencedirect.com/science/article/pii/S0376738816302204

[30] L. Dumée, S. Smart, M. C. Duke, S. R. Gray, Next generation membranes for membrane distillation and future prospects, 2015. doi:10.1016/B978-1-78242-246-4.00014-3.
URL http://linkinghub.elsevier.com/retrieve/pii/B9781782422464000143

[31] M. I. Ali, E. K. Summers, H. A. Arafat, J. H. Lienhard V, Effects of membrane properties on water production cost in small scale membrane distillation systems, Desalination 306 (2012) 60 – 71. doi:10.1016/j.desal.2012.07.043.
URL http://www.sciencedirect.com/science/article/pii/S0011916412004262

[32] A. Alklaibi, N. Lior, Transport analysis of air-gap membrane distillation, Journal of Membrane Science 255 (1-2) (2005) 239–253. doi:10.1016/j.memsci.2005.01.038.
URL http://linkinghub.elsevier.com/retrieve/pii/S0376738805001171

[33] H. Yu, X. Yang, R. Wang, A. G. Fane, Numerical simulation of heat and mass transfer in direct membrane distillation in a hollow fiber module with laminar flow, Journal of Membrane Science 384 (1-2) (2011) 107–116. doi:10.1016/j.memsci.2011.09.011.
URL https://www.engineeringvillage.com/blog/document.url?mid=cpx_134e4fb1331e235327M73c42061377553&database=cpx

[34] B. Li, K. K. Sirkar, Novel membrane and device for vacuum membrane distillation-based desalination process, Journal of Membrane Science 257 (2005) 60–75. doi:10.1016/j.memsci.2004.08.040.
URL http://www.sciencedirect.com/science/article/pii/S0376738804008452

[35] M. Qtaishat, T. Matsuura, B. Kruczek, M. Khayet, Heat and mass transfer analysis in direct contact membrane distillation, Desalination 219 (1-3) (2008) 272–292. doi:10.1016/j.desal.2007.05.019.
URL http://www.sciencedirect.com/science/article/pii/S0011916407005826

[36] S. Al-Obaidani, E. Curcio, F. Macedonio, G. Di Profio, H. Al-Hinai, E. Drioli, Potential of membrane distillation in seawater desalination: Thermal efficiency, sensitivity study and cost estimation, Journal of Membrane Science 323 (1) (2008) 85–98. doi:10.1016/j.memsci.2008.06.006.
URL http://www.sciencedirect.com/science/article/pii/S0376738808005577

[37] Z. Li, Y. Peng, Y. Dong, H. Fan, P. Chen, L. Qiu, Q. Jiang, Effects of thermal efficiency in DCMD and the preparation of membranes with low thermal conductivity, Applied Surface Science 317 (2014)

338–349. doi:10.1016/j.apsusc.2014.07.080.
URL https://www.engineeringvillage.com/blog/document.url?mid=cpx_433659da149ab18cca6M642310178163125&database=cpx

[38] J. Phattaranawik, R. Jiraratananon, a. G. Fane, Heat transport and membrane distillation coefficients in direct contact membrane distillation, Journal of Membrane Science 212 (1-2) (2003) 177–193. doi:10.1016/S0376-7388(02)00498-2.
URL http://www.sciencedirect.com/science/article/pii/S0376738802004982

[39] P. Termpiyakul, R. Jiraratananon, S. Srisurichan, Heat and mass transfer characteristics of a direct contact membrane distillation process for desalination, Desalination 177 (1-3) (2005) 133–141. doi:10.1016/j.desal.2004.11.019.
URL http://www.sciencedirect.com/science/article/pii/S0011916405001864

[40] H. Lee, F. He, L. Song, J. Gilron, K. K. Sirkar, Desalination with a cascade of cross-flow hollow fiber membrane distillation devices integrated with a heat exchanger, AlChE Journal 57 (7) (2011) 1780–1795. doi:10.1002/aic.12409.
URL http://onlinelibrary.wiley.com/doi/10.1002/aic.12409/abstract

[41] A. Alklaibi, N. Lior, Comparative Study of Direct Contact and Air Gap Membrane Distillation Processes, Ind. Eng. Chem. Res 2 (46) (2007) 584–590. doi:10.1021/ie051094u.
URL http://pubs.acs.org/doi/abs/10.1021/ie051094u

[42] L. Martínez, J. M. Rodríguez-Maroto, On transport resistances in direct contact membrane distillation, Journal of Membrane Science 295 (1-2) (2007) 28–39. doi:10.1016/j.memsci.2007.02.029.
URL http://www.sciencedirect.com/science/article/pii/S0376738807001299

[43] L. Eykens, I. Hitsov, K. De Sitter, C. Dotremont, L. Pinoy, I. Nopens, B. Van der Bruggen, Influence Of Membrane Thickness And Process Conditions On Direct Contact Membrane Distillation At Different Salinities, Journal of Membrane Science 498 (2015) 353–364. doi:10.1016/j.memsci.2015.07.037.
URL http://linkinghub.elsevier.com/retrieve/pii/S0376738815300661

[44] A. Fane, R. Schofield, C. Fell, The efficient use of energy in membrane distillation, Desalination 64 (1987) 231–243. doi:10.1016/0011-9164(87)90099-3.
URL http://www.sciencedirect.com/science/article/pii/0011916487900993

[45] J. Koschikowski, M. Wieghaus, M. Rommel, Solar thermal-driven desalination plants based on membrane distillation, Desalination 156 (1-3) (2003) 295–304. doi:10.1016/S0011-9164(03)00360-6.
URL http://www.sciencedirect.com/science/article/pii/S0011916403003606

[46] G. P. Thiel, R. K. McGovern, S. M. Zubair, J. H. Lienhard V, Thermodynamic equipartition for increased second law efficiency, Applied Energy 118 (2014) 292–299. doi:10.1016/j.apenergy.2013.12.033.
URL http://www.sciencedirect.com/science/article/pii/S0306261913010325

[47] J. Swaminathan, H. W. Chung, D. M. Warsinger, J. H. Lienhard V, Simple method for balancing direct contact membrane distillation, Desalination 383 (2016) 53 – 59. doi:10.1016/j.desal.2016.01.014.
URL http://www.sciencedirect.com/science/article/pii/S0011916416300133

[48] K. H. Mistry, A. Mitsos, J. H. Lienhard V, Optimal operating conditions and configurations for humidification–dehumidification desalination cycles, International Journal of Thermal Sciences 50 (5) (2011) 779–789. doi:10.1016/j.ijthermalsci.2010.12.013.
URL http://linkinghub.elsevier.com/retrieve/pii/S129007291000356X

[49] K. H. Mistry, J. H. Lienhard V, Generalized Least Energy of Separation for Desalination and Other Chemical Separation Processes, Entropy 15 (6) (2013) 2046–2080. doi:10.3390/e15062046.
URL http://www.mdpi.com/1099-4300/15/6/2046

[50] M. H. Sharqawy, J. H. Lienhard V, S. M. Zubair, Thermophysical properties of seawater: A review of existing correlations and data, Desalination and Water Treatment 16 (2010) 354–380. doi:10.5004/dwt.2010.1079.
URL http://web.mit.edu/lienhard/www/Thermophysical_properties_of_seawater-DWT-16-354-2010.pdf

[51] K. G. Nayar, M. H. Sharqawy, L. D. Banchik, J. H. Lienhard V, Thermophysical properties of seawater: A review and new correlations that include pressure dependence, Desalination 390 (2016) 1–24. doi:10.1016/j.desal.2016.02.024.
URL http://www.sciencedirect.com/science/article/pii/S0011916416300807

[52] K. H. Mistry, R. K. McGovern, G. P. Thiel, E. K. Summers, S. M. Zubair, J. H. Lienhard V, Entropy Generation Analysis of Desalination Technologies, Entropy 13 (10) (2011) 1829–1864. doi:10.3390/e13101829.
URL http://www.mdpi.com/1099-4300/13/10/1829/

[53] J. H. Lienhard V, J. H. Lienhard IV, A Heat Transfer Textbook, Fourth Edition, Dover Publications, Inc, 2011.
URL http://ahtt.mit.edu

[54] L. D. Banchik, M. H. Sharqawy, J. H. Lienhard V, Effectiveness–mass transfer units (ε–MTU) model of a reverse osmosis membrane mass exchanger, Journal of Membrane Science 458 (2014) 189–198. doi:10.1016/j.memsci.2014.01.039.
URL http://www.sciencedirect.com/science/article/pii/S0376738814000520

[55] M. H. Sharqawy, L. D. Banchik, J. H. Lienhard V, Effectiveness–mass transfer units (ε–MTU) model of an ideal pressure retarded osmosis membrane mass exchanger, Journal of Membrane Science 445 (2013) 211–219. doi:10.1016/j.memsci.2013.06.027.
URL http://www.sciencedirect.com/science/article/pii/S0376738813005206

[56] S.A.Klein, Engineering Equation Solver.
URL http://www.fchart.com/ees/

[57] E. K. Summers, J. H. Lienhard V, Experimental study of thermal performance in air gap membrane distillation systems, including the direct solar heating of membranes, Desalination 330 (2013) 100–111. doi:10.1016/j.desal.2013.09.023.
URL http://www.sciencedirect.com/science/article/pii/S0011916413004554

[58] D. Winter, Membrane distillation: A thermodynamic, technological and economic analysis, Ph.D. thesis, University of Kaiserslautern, Germany (2015).
URL http://www.reiner-lemoine-stiftung.de/pdf/dissertationen/Dissertation-Winter.pdf